Inorganic Chemistry

Article

pubs.acs.org/IC

Emissive {Mn^{III}_4Ca} Clusters with Square Pyramidal Topologies: Syntheses and Structural, Spectroscopic, and Physicochemical Characterization

Alysha A. Alaimo,[†] Daisuke Takahashi,[‡] Luís Cunha-Silva,[§] George Christou,[‡] and Theocharis C. Stamatatos*,[†]

[†]Department of Chemistry, Brock University, St. Catharines L2S 3A1, Ontario, Canada

[‡]Department of Chemistry, University of Florida, Gainesville, Florida 32611-7200, United States

[§]REQUIMTE & Department of Chemistry and Biochemistry, Faculty of Sciences, University of Porto, 4169-007 Porto, Portugal

Supporting Information

ABSTRACT: The one-pot reactions between $Mn(ClO_4)_2\cdot 6H_2O$, $Ca(ClO_4)_2\cdot 4H_2O$, and the potentially tetradentate (N,O,O,O) chelating/bridging ligand salicylhydroxime ($shiH_3$), resulting from the in situ metal ion-assisted amide−iminol tautomerism of salicylhydroxamic acid in the presence of various fluorescence carboxylate groups and base NEt_3, afford a family of structurally similar {Mn_4Ca} clusters with distorted square pyramidal topology. The reported complexes $(NHEt_3)_2[Mn_4Ca(L1)_4(shi)_4]$ (**1**), $(NHEt_3)_2[Mn_4Ca(L2)_4(shi)_4]$ (**2**), $(NHEt_3)_5[Mn_4Ca(L2)_4(shi)_4(shiH_2)_2](ClO_4)$ (**3**), and $(NHEt_3)_2[Mn_4Ca(L3)_4(shi)_4]$ (**4**) contain a similar $[Mn_4Ca(\mu\text{-}NO)_4]^{10+}$ core of four Mn^{III} atoms at the square base and a Ca^{II} atom occupying the apical site. Peripheral ligation about the core is provided by four $\eta^1{:}\eta^1{:}\mu$ carboxylate groups of the anions of 2-naphthoic acid ($L1^-$), 9-anthracenecarboxylic acid ($L2^-$), and 1-pyrenecarboxylic acid ($L3^-$). Solid-state direct current magnetic susceptibility studies revealed the presence of predominant antiferromagnetic exchange interactions between the 4 Mn^{III} centers, which were primarily quantified by using a simple 1-J fit model to give $S = 0$ spin ground states with low-lying excited states close in energy to the ground state. Solution studies in solvent MeCN were carried out on all complexes and confirmed their structural integrity. Cyclic voltammetry studies showed a similar well-defined reversible oxidation and an irreversible reduction for all complexes, thus establishing their redox potency and electrochemical efficiency. Emission studies in solution proved the optical activity of all compounds, with the observed "blue" emission peaks attributed to the π-rich chromophores of the organic fluorescence ligands. The combined results demonstrate the ability of $shiH_3$ and fluorescence carboxylates to yield new heterometallic Mn/Ca clusters with (i) the same Mn/Ca ratio as the oxygen-evolving complex of Photosystem II, (ii) structural stability in solution, and (iii) a pronounced redox and optical activity.

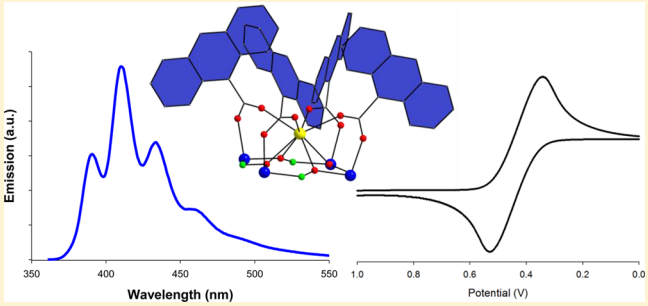

INTRODUCTION

Photosynthesis is the sunlight-driven process by which green plants, algae, and cyanobacteria convert CO_2 and H_2O into carbohydrates and molecular O_2.[1] Such a light-powered process is responsible for essentially all the O_2 on this planet. Photosystem II (PSII) is a multicomponent assembly of proteins and cofactors that absorbs four photons to sequentially oxidize a {Mn_4CaO_5} cluster compound (Scheme 1),[2] known as the water-oxidizing complex (WOC) or the oxygen-evolving complex (OEC), through a four-electron process called the Kok cycle.[3] The latter involves a sequence of the so-called S_n Kok states (n = 0 to 4) with the most oxidized one, S_4, participating to the O_2 release and the S_1 being dubbed as the dark-adapted or dark-stable state.[4] Although still of some debate,[5] the Mn ions at the various S_n Kok states all exist in high oxidation states and are assigned as a mixture of Mn^{III}, Mn^{IV}, and probably Mn^{V}; the S_0 state is $3Mn^{III},Mn^{IV}$, the dark-stable S_1 state is $2Mn^{III},2Mn^{IV}$, the S_2, the most studied Kok state, is $Mn^{III},3Mn^{IV}$, and the S_4 is either a $4Mn^{IV}$-ligand radical description or a $3Mn^{IV},Mn^{V}$ state.[6] In addition, the presence of Ca^{2+} ion is vital for the WOC activity; without its existence the

Scheme 1. {Mn_4CaO_5} Core of the Oxygen-Evolving Complex in Photosystem II

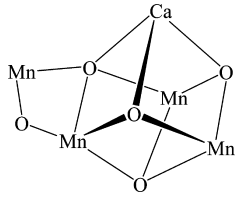

Received: October 11, 2014
Published: December 5, 2014

   dx.doi.org/10.1021/ic502492x | Inorg. Chem. 2015, 54, 2137−2151

OEC could not advance to the S_3 state.[7] The assembly of the four Mn and one Ca^{2+} ions in the active site of PSII is achieved via a combination of μ-, μ_3-, and μ_4-O^{2-} groups, which give rise to the formation of an oxido-bridged $\{Mn_3CaO_4\}$ distorted cubane linked to a fourth, "dangling" Mn atom (Scheme 1).[8] Peripheral ligation about the Mn_4CaO_5 core is primarily provided by aspartate and glutamate carboxylate groups of various polypeptide moieties. It becomes apparent that the presence of oxido groups is of significant importance for the stabilization of the higher Mn oxidation states and simultaneously for the satisfaction of the Ca^{2+} oxophilicity. Oxides can be generated from the complete deprotonation of water molecules; the process by which the OEC is assembled, called photoactivation, utilizes Mn, Ca, Cl^-, H_2O, and oxidizing equivalents that result from light absorption.[9] Despite the large number of multinuclear, homometallic Mn clusters that have been synthesized at various high oxidation states,[10] heterometallic Mn^{n+}–Ca cluster chemistry has been only sparingly explored.[11−13] Agapie and co-workers,[12] and some of us,[13] have reported the two closest to the overall topology of native OEC inorganic model complexes, both containing a $\{Mn_3CaO_4\}$ cubane core with all Mn atoms in the high oxidation state of 4+.

Kinetically distinct species in photoactivation process have been established,[14] and reduction of the S_n intermediates in the Kok cycle has led to species in oxidation states lower than S_0, which do not require the presence of oxido groups; these S_n states ($n = -1, -2, -3$) are known as the reduced OEC states and contain Mn ions in oxidation states ≤ 3.[15] For instance, the S_{-3} state corresponds to a putative Mn^{II},$3Mn^{III}$ oxidation state.[16] During the catalytic turnover, lower oxidation state species with lower oxygen-atom content must be generated upon loss of molecular O_2. The ligand set environment is then responsible for the periodic reorganization, reoxidation, and reoxygenation of the Mn_4CaO_x cluster.[17] Thus, the synthesis and detailed study of synthetic analogues (molecular models) of such lower oxidation state species would greatly enhance our understanding of the spectroscopic, physical, and catalytical properties of the WOC, as well as its reactivity and functional characteristics. In addition, the incorporation of optically active organic groups in an inorganic Mn_4Ca core could provide access to additional physical properties such as luminescence and photocatalysis.

Toward the search for new molecular materials with implications in both bioinorganic chemistry and materials science, and specifically in the synthesis of structural models of OEC with optical properties, some of the most crucial synthetic challenges to confront are (i) the Mn_4Ca metal stoichiometry, (ii) the extended, distorted cubane conformation, (iii) the stability of the preferred Mn oxidation states, (iv) the choice of the ancillary bridging ligands, and (v) the optical response to an external stimulus. With this in mind, we started a program aiming at the synthesis of new heterometallic Mn–Ca clusters that would possess as many of the above-mentioned structural and physicochemical features as possible.[18] The synthetic route employed was based on self-assembly, which includes one-pot reactions between various Mn and Ca sources in the presence of carefully selected organic chelating/bridging ligands. With regard to the choice of organic ligands, Pecoraro and co-workers[19] have elegantly shown that salicylhydroxamic acid ($shaH_2$, Scheme 2) can potentially undergo a metal-assisted amide–iminol tautomerism, which leads to salicylhydroxime ($shiH_3$, Scheme 2); the latter is an oximate-based ligand with four coordination sites available for binding to both Mn and Ca metal centers. Oximate-based ligands (>C=N–O^-) are known to stabilize Mn atoms with moderate-to-high oxidation states, also fostering the formation of polynuclear metal complexes.[20] In addition, carboxylate groups with fluorescence substituents, such as naphthalene, anthracene, and pyrene (Scheme 2, bottom),[21] can potentially provide ancillary ligation to an inorganic metal core and simultaneously introduce optical efficiency into the corresponding cluster compounds. We have recently shown that the employment of 2-naphthoic acid (L1-H), 9-anthracenecarboxylic acid (L2-H), and 1-pyrenecarboxylic acid (L3-H) in Mn^{III} cluster chemistry can lead to a family of $[Mn^{III}_3O(LX)_3(mpko)_3](ClO_4)$ triangular clusters (X = 1, 2, or 3; $mpko^-$ is the anion of methyl 2-pyridyl ketone oxime) with dual single-molecule magnetic and emissive properties.[22] Interestingly, the photoluminescence induced by the fluorescence ligands was not quenched by the highly paramagnetic nature of the metal complexes.

Scheme 2. Structural Formulae and Abbreviations of the Organic Ligands Used in this Study

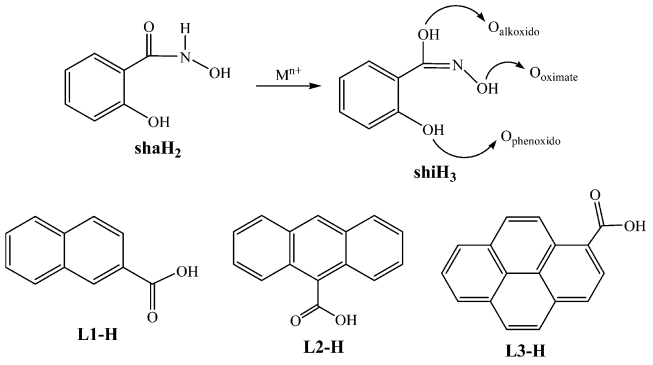

We here report the synthesis and structural, spectroscopic, and physicochemical properties of a new family of oxido-free $\{Mn^{III}_4Ca\}$ clusters with some relevance to low oxidation states of OEC, featuring a distorted square pyramidal topology, an inherent structural stability in solution, and redox and optical activities arising from the metal ions and fluorescence ligands.

EXPERIMENTAL SECTION

Synthesis. All manipulations were performed under aerobic conditions using chemicals and solvents as received.

*$(NHEt_3)_2[Mn_4Ca(L1)_4(shi)_4]$ (**1**).* To a stirred, colorless solution of $shaH_2$ (0.15 g, 1.0 mmol) and NEt_3 (0.42 mL, 3.0 mmol) in CH_2Cl_2 (30 mL) was added solid 2-naphthoic acid (L1-H; 0.17 g, 1.0 mmol). The resulting pale yellow suspension was kept under magnetic stirring at room temperature for ~10 min, followed by the consecutive addition of solids $Mn(ClO_4)_2{\cdot}6H_2O$ (0.16 g, 0.5 mmol) and $Ca(ClO_4)_2{\cdot}4H_2O$ (0.16 g, 0.5 mmol). The resulting ecru suspension was stirred for 2 h, during which time all the solids dissolved, and the color of the solution changed to dark brown. The solution was filtered, and a mixture of Et_2O/C_6H_{14} (60 mL, 1:1 v/v) diffused into the filtrate. After 5 d, brown platelike crystals of **1** had appeared and were collected by filtration, washed with CH_2Cl_2 (2 × 5 mL) and Et_2O (2 × 5 mL), and dried under vacuum; the yield was 30%. The crystalline solid was analyzed as **1**: C, 57.67; H, 4.38; N, 4.80%. Found: C, 57.43; H, 4.25; N, 4.99%. Selected attenuated total reflection (ATR) data (cm^{-1}): 3050 (wb), 2985 (m), 1595 (vs), 1565 (s), 1509 (m), 1467 (m), 1432 (s), 1388 (m), 1315 (m), 1244 (m), 1153 (m), 1097 (m), 1033 (s), 937 (m), 863 (m), 792 (m), 753 (mb), 681 (s), 648 (mb), 480 (m). UV–vis: λ/nm in MeCN: 243, 270, 331.

*$(NHEt_3)_2[Mn_4Ca(L2)_4(shi)_4]$ (**2**).* To a stirred, colorless solution of $shaH_2$ (0.15 g, 1.0 mmol) and NEt_3 (0.56 mL, 4.0 mmol) in CH_2Cl_2 (30 mL) was added solid 9-anthracenecarboxylic acid (L2-H; 0.18 g,

dx.doi.org/10.1021/ic502492x | Inorg. Chem. 2015, 54, 2137−2151

Table 1. Crystallographic Data for Complexes 1−4

parameter	**1**	**2**·4CH_2Cl_2	**3**·2CH_2Cl_2	**4**·5CH_2Cl_2
formula[a]	$C_{84}H_{76}Mn_4CaN_6O_{20}$	$C_{104}H_{92}Mn_4CaN_6O_{20}Cl_8$	$C_{134}H_{148}Mn_4CaN_{11}O_{30}Cl_5$	$C_{113}H_{94}Mn_4CaN_6O_{20}Cl_{10}$
FW[a]/g mol^{-1}	1749.35	2289.28	2829.72	2470.28
crystal type	brown plate	brown plate	brown plate	red plate
crystal size/mm	0.35 × 0.18 × 0.05	0.38 × 0.21 × 0.11	0.25 × 0.14 × 0.03	0.08 × 0.05 × 0.03
crystal system	orthorhombic	monoclinic	monoclinic	triclinic
space group	*Pbcn*	$P2_1/n$	$P2_1/n$	$P\bar{1}$
a/Å	17.774(2)	21.872(2)	14.7076(12)	16.5865(2)
b/Å	26.125(4)	19.242(2)	29.524(2)	17.4560(2)
c/Å	17.139(2)	26.024(2)	31.846(2)	19.3789(3)
α/deg	90	90	90	110.620(1)
β/deg	90	91.153(4)	101.206(3)	94.871(1)
γ/deg	90	90	90	94.214(1)
V/Å^3	7958.4(2)	10950.2(16)	13564.8(2)	5200.2(1)
Z	4	4	4	1
T/K	150.0(2)	150.0(2)	150.0(2)	100(2)
ρ_{calc}/g cm^{-3}	1.460	1.389	1.386	1.578
μ/mm^{-1}	0.762	0.760	0.577	0.771
θ range/deg	3.65−25.03	3.65−25.03	3.66−25.03	3.52−23.97
index ranges	$0 \le h \le 21$	$-25 \le h \le 26$	$-17 \le h \le 17$	$-19 \le h \le 19$
	$0 \le k \le 31$	$-22 \le k \le 22$	$-35 \le k \le 35$	$-20 \le k \le 20$
	$0 \le l \le 20$	$-30 \le l \le 30$	$-37 \le l \le 37$	$-22 \le l \le 20$
collected reflections	6968	139 672	168 834	54 493
independent reflections	4534 (R_{int} = 0.1645)	19 125 (R_{int} = 0.0476)	23 889 (R_{int} = 0.0765)	15 587 (R_{int} = 0.0307)
final $R^{b,c}$ indices [$I > 2\sigma(I)$]	$R1$ = 0.1554	$R1$ = 0.0925	$R1$ = 0.0969	$R1$ = 0.0784
	$wR2$ = 0.4217	$wR2$ = 0.2370	$wR2$ = 0.1991	$wR2$ = 0.2322
$(\Delta\rho)_{max,min}$/e Å^{-3}	4.111, −0.713	3.599, −1.200	1.799, −1.188	1.897, −1.613

[a]Including solvate molecules. [b]$R1 = \Sigma(||F_o| - |F_c||)/\Sigma|F_o|$. [c]$wR2 = [\Sigma[w(F_0^2 - F_c^2)^2]/\Sigma[w(F_0^2)^2]]^{1/2}$, $w = 1/[\sigma^2(F_0^2) + (ap)^2 + bp]$, where $p = [\max(F_0^2, 0) + 2F_c^2]/3$.

0.8 mmol). The resulting pale yellow suspension was kept under magnetic stirring at room temperature for ∼15 min, followed by the consecutive addition of solids $Mn(ClO_4)_2{\cdot}6H_2O$ (0.29 g, 0.8 mmol) and $Ca(ClO_4)_2{\cdot}4H_2O$ (0.06 g, 0.2 mmol). The resulting ecru suspension was stirred for 2 h, during which time all the solids dissolved, and the color of the solution changed to dark brown. The solution was filtered, and Et_2O (60 mL) diffused into the filtrate. After 3 d, X-ray quality dark brown platelike crystals of **2**·4CH_2Cl_2 had appeared and were collected by filtration, washed with CH_2Cl_2 (2 × 5 mL) and Et_2O (2 × 5 mL), and dried under vacuum; the yield was 60%. The crystalline solid was analyzed as **2**: C, 61.61; H, 4.34; N, 4.31%. Found: C, 61.39; H, 4.25; N, 4.34%. Selected ATR data (cm^{-1}): 3041 (m), 2983 (m), 1589 (vs), 1565 (s), 1513 (m), 1486 (m), 1468 (m), 1429 (s), 1384 (m), 1313 (vs), 1274 (m), 1254 (m), 1154 (m), 1096 (m), 1031 (m), 937 (s), 884 (m), 861 (s), 797 (m), 733 (vs), 681 (s), 646 (s), 615 (vs), 524 (m), 481 (m), 457 (m). UV−vis: λ/nm in MeCN: 250, 288, 347, 356, 382.

$(NHEt_3)_5[Mn_4Ca(L2)_4(shi)_4(shiH_2)_2](ClO_4)$ (**3**). To a stirred, colorless solution of $shaH_2$ (0.05 g, 0.3 mmol) and NEt_3 (0.13 mL, 0.9 mmol) in CH_2Cl_2 (30 mL) was added solid 9-anthracenecarboxylic acid (L2-H; 0.07 g, 0.3 mmol). The resulting pale yellow suspension was kept under magnetic stirring at room temperature for ∼15 min, followed by the consecutive addition of solids $Mn(ClO_4)_2{\cdot}6H_2O$ (0.11 g, 0.3 mmol) and $Ca(ClO_4)_2{\cdot}4H_2O$ (0.06 g, 0.2 mmol). The resulting ecru suspension was stirred for 2 h, during which time all the solids dissolved, and the color of the solution changed to dark brown. The solution was filtered, and a mixture of Et_2O/C_6H_{14} (60 mL, 1:1 v/v) diffused into the filtrate. After four weeks, dark red platelike crystals of **3**·2CH_2Cl_2 appeared and were collected by filtration, washed with CH_2Cl_2 (2 × 5 mL) and Et_2O (2 × 5 mL), and dried under vacuum; the yield was 20%. The crystalline solid was analyzed as solvent-free **3**: C, 60.28; H, 5.75; N, 6.92%. Found: C, 60.10; H, 5.52; N, 7.12%. Selected ATR data (cm^{-1}): 3040 (s), 2981 (mb), 1593 (vs), 1567 (s), 1515 (m), 1431(s), 1383 (m), 1311 (vs), 1256 (m), 1155 (m), 1093 (m), 1032 (m), 1024 (s), 936 (m), 898 (m), 861 (s), 756 (s), 734 (s), 679 (s), 647 (s), 619 (vs), 524 (m), 478 (m), 456 (m). UV−vis: λ/nm in MeCN: 252, 284, 350, 358, 381.

$(NHEt_3)_2[Mn_4Ca(L3)_4(shi)_4]$ (**4**). To a stirred, colorless solution of $shaH_2$ (0.15 g, 1.0 mmol) and NEt_3 (0.56 mL, 4.0 mmol) in CH_2Cl_2 (30 mL) was added solid 1-pyrenecarboxylic acid (L3-H; 0.20 g, 0.8 mmol). The resulting pale yellow suspension was kept under magnetic stirring at room temperature for ∼15 min, followed by the consecutive addition of solids $Mn(ClO_4)_2{\cdot}6H_2O$ (0.29 g, 0.8 mmol) and $Ca(ClO_4)_2{\cdot}4H_2O$ (0.06 g, 0.2 mmol). The resulting ecru suspension was stirred for 2 h, during which time all the solids dissolved, and the color of the solution changed to dark brown. The solution was filtered and left to evaporate slowly at room temperature. After 5 d, X-ray quality dark brown platelike crystals of **4**·5CH_2Cl_2 appeared and were collected by filtration, washed with CH_2Cl_2 (2 × 5 mL) and Et_2O (2 × 5 mL), and dried under vacuum; the yield was 50%. The crystalline solid was analyzed as solvent-free **4**: C, 63.41; H, 4.14; N, 4.11%. Found: C, 63.76; H, 4.42; N, 3.98%. Selected ATR data (cm^{-1}): 3035 (m), 2984 (m), 1591 (vs), 1567 (s), 1510 (m), 1469 (m), 1432 (s), 1386 (m), 1353 (s), 1311 (m), 1255 (m), 1178 (m), 1152 (m), 1095 (m), 1033 (s), 936 (s), 839 (s), 787 (m), 753 (m), 712 (vs), 678 (vs), 645 (m), 612 (vs), 533 (m), 479 (s). UV−vis: λ/nm in MeCN: 250, 288, 342, 360, 382.

X-ray Crystallography. Selected crystals of **1**·2H_2O, **2**·4CH_2Cl_2, and **3**·2CH_2Cl_2 were manually harvested and mounted on cryoloops using adequate oil.[23] Diffraction data were collected at 150.0(2) K on a Bruker X8 Kappa APEX II charge-coupled device (CCD) area-detector diffractometer controlled by the APEX2 software package[24] (Mo Kα graphite-monochromated radiation, λ = 0.710 73 Å), and equipped with an Oxford Cryosystems Series 700 cryostream monitored remotely with the software interface Cryopad.[25] Images were processed with the software SAINT+.[26] The majority of single crystals chosen for data collection showed very weak X-ray diffraction patterns under Mo Kα radiation; it was not feasible to obtain any better data for complexes **1**−**3** than the ones reported herein. Attempts to work with larger crystals failed to give acceptable data due

dx.doi.org/10.1021/ic502492x | Inorg. Chem. 2015, 54, 2137−2151

to crystal twinning problems. To confirm that the intensity of conventional X-rays hinders the acquisition of high-quality crystal data, access to synchrotron radiation was necessary. Selectively for complex **4**·5CH_2Cl_2, good-quality X-ray diffraction data from a small, but single, crystal were collected under the synchrotron radiation beam at the Swiss-Norwegian BM01a beamline (European Synchrotron Radiation Facilities (ESRF), Grenoble, France), at 100(2) K, on the multipurpose PILATUS@SNBL diffractometer equipped with a PILATUS2m detector, using a highly monochromatic synchrotron radiation with wavelength (λ) fixed at 0.68239 Å. Images were processed using the software CrysAlis^{Pro}.[27] All the data were corrected for absorption by the multiscan semiempirical method implemented in SADABS.[28] The structures were solved by direct methods implemented in SHELXS-97[29,30] and refined from successive full-matrix least-squares cycles on F^2 using SHELXL-97.[30,31]

The non-hydrogen atoms were successfully refined using anisotropic displacement parameters, except from one Et_3NH^+ cation in the structures of **1** and **2**·4CH_2Cl_2, which were refined with isotropic parameters. Hydrogen atoms bonded to carbon, nitrogen, or oxygen atoms were located at their idealized positions using appropriate HFIX instructions in SHELXL; 43 for the aromatic carbons, 23 for the $-CH_2$ group, 137 for the terminal $-CH_3$ methyl groups, 13 for the $-NH$ group, and 147 for the $-OH$ group. All these atoms were included in subsequent refinement cycles in riding-motion approximation with isotropic thermal displacements parameters (U_{iso}) fixed at 1.2 or 1.5 × U_{eq} of the relative atom.

Substantial electron density was found on the data of **1**, **2**·4CH_2Cl_2, and **3**·2CH_2Cl_2, most likely as a consequence of additional disordered solvent molecules. Several attempts to locate and model remaining solvent molecules revealed to be ineffective, and the investigation for the total potential solvent area using the software package PLATON[32] confirmed unequivocally the occurrence of cavities with potential solvent-accessible void volume. Therefore, the original data sets were treated with the SQUEEZE[32c] subroutines to eliminate the contribution of these highly disordered molecules in the solvent-accessible volume. The programs used for molecular graphics were MERCURY and DIAMOND.[33] Unit cell parameters and structure solution and refinement data for all complexes are listed in Table 1. Further crystallographic details can be found in the corresponding CIF files provided in the Supporting Information.

Physical Measurements. Infrared (IR) spectra were recorded in the solid state on a Bruker FT-IR spectrometer (ALPHA Platinum ATR single reflection) in the 4000−450 cm^{-1} range. Elemental analyses (C, H, and N) were performed on a PerkinElmer 2400 Series II Analyzer. UV−visible (UV−vis) spectra were recorded in MeCN solution at concentrations ~10^{-5} M on a Beckman Coulter DU Series 700 dual beam spectrophotometer. Electrospray ionization (ESI) mass spectra (MS) were taken on a Bruker HCT Ultra mass spectrometer from solutions of complexes **1**−**4** prepared in MeCN. Excitation and emission spectra were recorded in MeCN solutions (~10^{-5} M) using a PTI FeliX32 spectrofluorometer. Electrochemical studies were performed under argon using a BASi EC-epsilon Autoanalyzer and a standard three-electrode assembly (glassy carbon working, Pt wire auxiliary, and $Ag/AgNO_3$ reference) with 0.1 M $NBu^n_4PF_6$ as supporting electrolyte. Quoted potentials are versus the ferrocene/ferrocenium couple, used as an internal standard. The scan rates for cyclic voltammetry were 100 mV/s. Distilled solvents were employed, and the concentrations of the complexes were approximately 1 mM. Direct current (dc) magnetic susceptibility studies were performed at the University of Florida Chemistry Department on a Quantum Design MPMS-XL SQUID susceptometer equipped with a 7 T magnet and operating in the 1.8−400 K range. Samples were embedded in solid eicosane to prevent torquing. Pascal's constants were used to estimate the diamagnetic correction, which was subtracted from the experimental susceptibility to give the molar paramagnetic susceptibility (χ_M).[34]

RESULTS AND DISCUSSION

Synthesis and IR Spectra. The majority of synthetic procedures to heterometallic Mn/Ca complexes rely on the reactions of readily available MnX_2 and CaX_2 starting materials (X^- = various) with a potentially chelating/bridging organic ligand. This route has led to numerous mixed Mn/Ca complexes with different metal stoichiometries, Mn oxidation level descriptions, and structural topologies.[11,12,35] An alternative route refers to the comproportionation reactions between Mn(II) and Mn(VII) reagents, in the presence of CaX_2 salts, under acidic conditions. This flexible and unpredictable strategy does not require the copresence of an organic chelate and has provided access to complex $[Mn^{IV}_3Ca_2O_4(O_2C^tBu)_8(^tBuCO_2H)_4]$,[13] one of the closest structural models of the asymmetric-cubane OEC unit. In the present study we followed the first route, and we have thus explored reactions involving salicylhydroxamic acid ($shaH_2$) chelate and Mn/Ca inorganic salts in the presence of various fluorescence carboxylate groups. The simultaneous presence of "competing" carboxylate groups (i.e., $MeCO_2^-$, $^tBuCO_2^-$, etc.) on the metal starting materials would likely complicate the reaction mixtures, and we have thus avoided their use.

A variety of reactions differing in the Mn/Ca/$shaH_2$ ratio, the fluorescence carboxylic acids, the inorganic ions present, the organic base, and/or the reaction solvent(s) were explored in identifying the following successful systems. The one-pot reaction of $Mn(ClO_4)_2·6H_2O$ and $Ca(ClO_4)_2·4H_2O$ with $shaH_2$ in a 1:1:2 molar ratio in CH_2Cl_2 in the presence of 2 and 6 equiv of each 2-naphthoic acid (L1-H) and NEt_3 gave a dark brown solution that, upon filtration and slow diffusion with Et_2O/hexanes, afforded brown crystals of the mixed-metal complex $(NHEt_3)_2[Mn^{III}_4Ca(L1)_4(shi)_4]$ (**1**) in 30% yield (based on the total available Ca). The formation of representative **1** is summarized in eq 1.

$$\begin{aligned} &4Mn(ClO_4)_2·6H_2O + Ca(ClO_4)_2·4H_2O + 4shiH_3 \\ &\quad + 4L1\text{-}H + O_2 + 12NEt_3 \\ &\rightarrow (NHEt_3)_2[Mn^{III}_4Ca(L1)_4(shi)_4] + 10(NHEt_3)(ClO_4) \\ &\quad + 30H_2O \end{aligned} \quad (1)$$

The coordinated anion of shi^{3-} was resulted from the metal ion-assisted transformation of $shaH_2$ under basic conditions. The reaction is an oxidation, undoubtedly by O_2 under the prevailing basic conditions. The NEt_3 has the role of proton acceptor to facilitate the deprotonation of the $shaH_2$ and L1-H molecules. Employment of different organic bases, such as NMe_3, Bu^n_3N and Me_4NOH, did not afford crystalline materials but only oily products that we were not able to further characterize. The reaction solvent was found to be of critical importance for the crystallization of all reported compounds **1**−**4**; various reactions in polar solvents gave amorphous precipitates that were probably mixtures of different products. Once the identity of **1** was established by single-crystal X-ray diffraction studies (vide infra), we managed to optimize the synthesis and increase the yield (~70%) of the crystalline compound by adjusting the Mn/Ca/$shaH_2$/L1-H/NEt_3 ratio to 4:1:5:4:20. The latter ratio was also adopted for the synthesis of isostructural compounds $(NHEt_3)_2[Mn_4Ca(L2)_4(shi)_4]$ (**2**) and $(NHEt_3)_2[Mn_4Ca(L3)_4(shi)_4]$ (**4**) in yields of 60 and 50%, respectively, under different crystallization methods (slow diffusion with Et_2O for **2** and slow evaporation at room

dx.doi.org/10.1021/ic502492x | Inorg. Chem. 2015, 54, 2137−2151

temperature for **4**). Interestingly, and only in case of 9-anthracenecarboxylic acid (L2-H), the metals-to-ligands ratio proved to slightly affect the chemical identity of $(NHEt_3)_2[Mn_4Ca(L\text{-}X)_4(shi)_4]$ (X = 1 (**1**), 2 (**2**), 3 (**4**)). Hence, the reaction of $Mn(ClO_4)_2\cdot 6H_2O$ and $Ca(ClO_4)_2\cdot 4H_2O$ with $shaH_2$ in a 3:2:3 molar ratio in CH_2Cl_2 in the presence of 3 and 9 equiv of each L2-H and NEt_3 gave a dark brown solution that, upon filtration and slow diffusion with Et_2O/hexanes, afforded brown crystals of $(NHEt_3)_5[Mn_4Ca(L2)_4(shi)_4(shiH_2)_2](ClO_4)$ (**3**) in 20% yield. The formation of **3** is summarized in eq 2.

$$\begin{aligned} &4Mn(ClO_4)_2\cdot 6H_2O + Ca(ClO_4)_2\cdot 4H_2O + 6shiH_3 \\ &\quad + 4L2\text{-}H + O_2 + 14NEt_3 \\ &\rightarrow (NHEt_3)_5[Mn_4Ca(L2)_4(shi)_4(shiH_2)_2](ClO_4) \\ &\quad + 9(NHEt_3)(ClO_4) + 30H_2O \end{aligned} \quad (2)$$

Complex **3** is again a $\{Mn_4Ca\}$ species albeit with two additional $shiH_2^-$ ions acting as terminal ligands (vide infra). Clearly, these reaction systems are very complicated, undoubtedly with many species in equilibrium, and thus are sensitive to small changes in reaction conditions. Finally, the substitution of ClO_4^- ions in the MnX_2 and CaX_2 precursors by other inorganic ions, such as Cl^- or NO_3^-, did not lead us to any crystalline material under various crystallization techniques and workup conditions. Compounds **1**−**4** are all stable and crystalline solids at room temperature and nonsensitive toward air and moisture. They are all soluble in MeCN, MeOH, dimethylformamide, and dimethyl sulfoxide and partially soluble in almost all other organic solvents such as benzene, tetrahydrofuran, and toluene. Given the pronounced ability of polar and protic solvents to reduce high-oxidation state Mn species,[36] we avoided dissolving the reported compounds in MeOH, and we have instead focused on the spectroscopic and physicochemical characterization of **1**−**4** in MeCN solutions.

All complexes **1**−**4** have very similar IR spectra. Several bands appear in the ∼1595−1380 cm^{-1} range, assigned to contributions from the stretching vibrations of the aromatic rings of shi^{3-} and fluorescence ligands, which overlap with stretches of the carboxylate bands;[37] they, thus, do not represent pure vibrations and render exact assignments difficult. Contributions from the $\nu(C{=}N)_{oximate}$ modes of shi^{3-} would be also expected in this region. It is very likely that the strong bands at 1595 and 1432 cm^{-1} (**1**), 1589 and 1429 cm^{-1} (**2**), 1593 and 1431 cm^{-1} (**3**), and 1591 and 1432 cm^{-1} (**4**) in the spectra of **1**−**4** are attributed to the $\nu_{as}(CO_2)$ and $\nu_s(CO_2)$ modes, respectively; the former should also involve a ring-stretching character. The difference Δ [$\Delta = \nu_{as}(CO_2) - \nu_s(CO_2)$] is small (<163 cm^{-1}) in all cases, as expected for the predominant bidentate bridging mode of carboxylate ligation (vide infra).[38] The bands at ∼3050 and ∼2980 cm^{-1} can be assigned to the stretching vibrations of ν(N−H) modes from the presence of Et_3NH^+ countercations.[39]

Description of Structures. Complexes **1**, **2**, and **4** are isostructural and differ only in the nature of the fluorescence carboxylate ligand and lattice solvate molecules; the latter will not be further discussed. Given the superior quality of X-ray diffraction data for compound **4** obtained through synchrotron radiation, and consequently its more precise metric parameters (bond distances and angles), only the structure of representative complex **4** will be described in detail. The crystal structure of **4** consists of a $[Mn_4Ca(L3)_4(shi)_4]^{2-}$ dianion (Figure 1, top), two Et_3NH^+ cations, and five lattice CH_2Cl_2 molecules. Complex **4**·5CH_2Cl_2 crystallizes in the triclinic space group $P\bar{1}$ with the $\{Mn_4Ca\}$ dianion in a general position. In contrast, complexes **1** (Figure 1, middle) and **2**·4CH_2Cl_2 (Figure 1, bottom) crystallize in the orthorhombic *Pbcn* and monoclinic

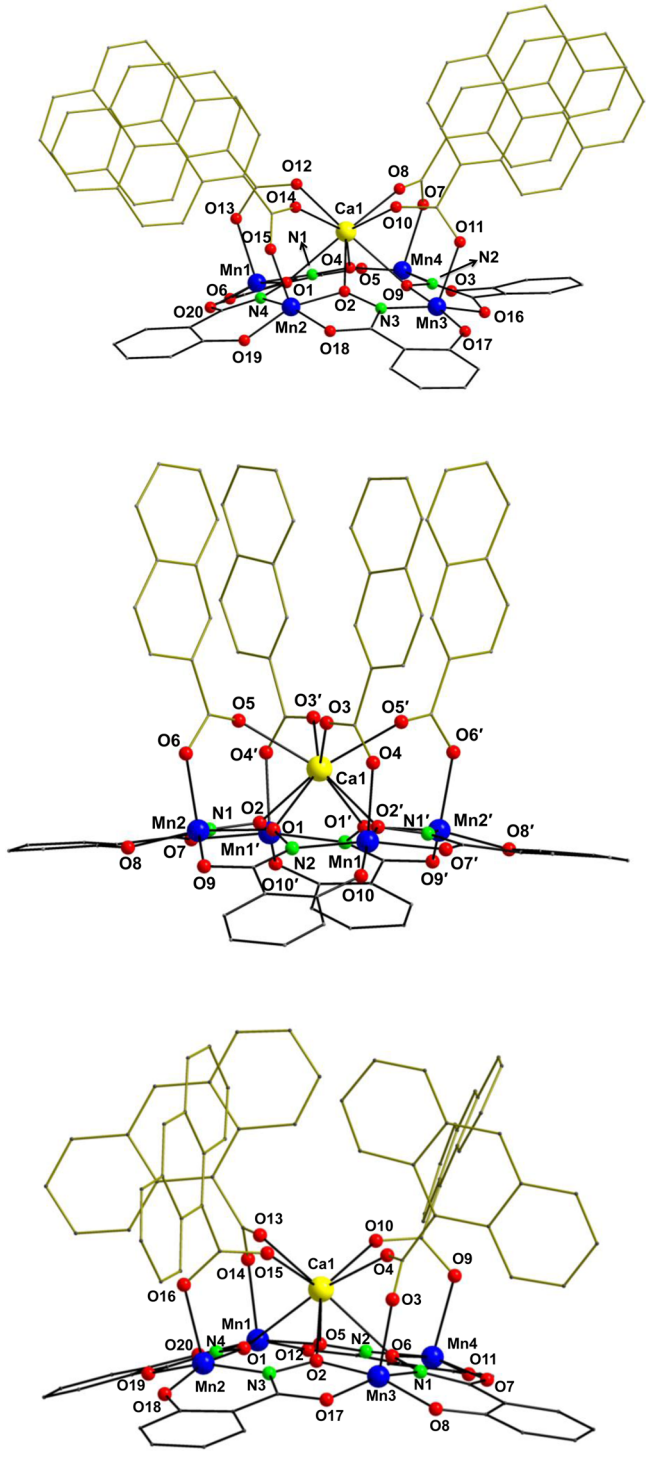

Figure 1. Partially labeled representations of the structures of the anions present in complexes **4** (top), **1** (middle), and **2** (bottom), with the gold thick bonds emphasizing the different carboxylate moieties. Color scheme: Mn^{III} blue, Ca^{II} yellow, O red, N green, C gray. H atoms are omitted for clarity. Symmetry operation for the primed atoms in **1**: $-x, y, 1/2 - z$.

dx.doi.org/10.1021/ic502492x | *Inorg. Chem.* 2015, 54, 2137−2151

Table 2. Selected Interatomic Distances (Å) and Angles (deg) for Complexes 1,[a] 2·4CH_2Cl_2, 3·2CH_2Cl_2, and 4·5CH_2Cl_2

1			
Mn(1)···Mn(2)	4.610(2)	Mn(2)···Mn(2′)	6.550(2)
Mn(1)···Mn(2′)	4.621(2)	Mn(1)···Ca(1)	3.678(2)
Mn(1)···Mn(1′)	6.495(2)	Mn(2)···Ca(1)	3.628(2)
Mn(1)−O(4)	2.122(7)	Mn(2)−O(1)	1.896(6)
Mn(1)−O(2′)	1.894(5)	Mn(2)−O(6)	2.050(7)
Mn(1)−O(7′)	1.974(7)	Mn(2)−O(8)	1.831(7)
Mn(1)−O(10)	1.839(6)	Mn(2)−O(9)	1.976(6)
Mn(1)−N(2)	1.933(6)	Mn(2)−N(1)	1.935(6)
Ca(1)−O(1)	2.376(6)	Ca(1)−O(3)	2.385(9)
Ca(1)−O(2)	2.353(5)	Ca(1)−O(5)	2.384(9)
Mn(1)−O(2′)−N(1′)−Mn(2′)	170.6	Mn(1′)−O(2)−Ca(1)	119.6(3)
Mn(2)−O(1)−N(2)−Mn(1)	174.1	Mn(2)−O(1)−Ca(1)	115.8(3)
2·4CH_2Cl_2			
Mn(1)···Mn(2)	4.612(1)	Mn(2)···Mn(4)	6.543(1)
Mn(2)···Mn(3)	4.630(1)	Mn(1)···Ca(1)	3.731(1)
Mn(3)···Mn(4)	4.636(1)	Mn(2)···Ca(1)	3.726(1)
Mn(4)···Mn(1)	4.615(1)	Mn(3)···Ca(1)	3.696(1)
Mn(1)···Mn(3)	6.533(1)	Mn(4)···Ca(1)	3.760(2)
Mn(1)−O(5)	1.880(4)	Mn(3)−O(2)	1.885(4)
Mn(1)−O(12)	1.944(4)	Mn(3)−O(3)	2.146(5)
Mn(1)−O(14)	2.069(5)	Mn(3)−O(8)	1.859(4)
Mn(1)−O(20)	1.860(4)	Mn(3)−O(17)	1.945(4)
Mn(1)−N(4)	1.963(5)	Mn(3)−N(1)	1.976(5)
Mn(2)−O(1)	1.868(4)	Mn(4)−O(6)	1.881(4)
Mn(2)−O(16)	2.115(4)	Mn(4)−O(7)	1.944(4)
Mn(2)−O(18)	1.862(4)	Mn(4)−O(9)	2.140(5)
Mn(2)−O(19)	1.947(4)	Mn(4)−O(11)	1.867(4)
Mn(2)−N(3)	1.974(5)	Mn(4)−N(2)	1.968(5)
Ca(1)−O(1)	2.466(4)	Ca(1)−O(6)	2.476(4)
Ca(1)−O(2)	2.428(4)	Ca(1)−O(10)	2.365(4)
Ca(1)−O(4)	2.405(4)	Ca(1)−O(13)	2.350(5)
Ca(1)−O(5)	2.503(4)	Ca(1)−O(15)	2.389(4)
Mn(1)−O(5)−N(2)−Mn(4)	179.2	Mn(1)−O(5)−Ca(1)	115.9(2)
Mn(2)−O(1)−N(4)−Mn(1)	177.0	Mn(2)−O(1)−Ca(1)	117.9(2)
Mn(3)−O(2)−N(3)−Mn(2)	175.0	Mn(3)−O(2)−Ca(1)	117.4(2)
Mn(4)−O(6)−N(1)−Mn(3)	175.6	Mn(4)−O(6)−Ca(1)	118.7(2)
3·2CH_2Cl_2			
Mn(1)···Mn(2)	4.617(3)	Mn(2)···Mn(4)	6.407(3)
Mn(2)···Mn(3)	4.569(2)	Mn(1)···Ca(1)	3.749(1)
Mn(3)···Mn(4)	4.641(3)	Mn(2)···Ca(1)	3.790(1)
Mn(4)···Mn(1)	4.535(2)	Mn(3)···Ca(1)	3.744(1)
Mn(1)···Mn(3)	6.566(5)	Mn(4)···Ca(1)	3.752(1)
Mn(1)−O(5)	1.875(4)	Mn(3)−O(2)	1.870(4)
Mn(1)−O(15)	1.951(4)	Mn(3)−O(3)	2.088(4)
Mn(1)−O(17)	2.158(4)	Mn(3)−O(8)	1.861(4)
Mn(1)−O(23)	1.851(4)	Mn(3)−O(20)	1.942(4)
Mn(1)−N(5)	1.970(5)	Mn(3)−N(1)	1.989(5)
Mn(2)−O(1)	1.893(4)	Mn(4)−O(6)	1.890(4)
Mn(2)−O(19)	2.283(4)	Mn(4)−O(7)	1.941(4)
Mn(2)−O(21)	1.873(4)	Mn(4)−O(9)	2.309(4)
Mn(2)−O(22)	1.961(4)	Mn(4)−O(11)	2.270(4)
Mn(2)−O(24)	2.244(4)	Mn(4)−O(14)	1.869(4)
Mn(2)−N(4)	1.976(5)	Mn(4)−N(3)	1.980(5)
Ca(1)−O(1)	2.468(4)	Ca(1)−O(6)	2.452(4)
Ca(1)−O(2)	2.440(4)	Ca(1)−O(10)	2.354(4)
Ca(1)−O(4)	2.397(4)	Ca(1)−O(16)	2.427(4)
Ca(1)−O(5)	2.399(4)	Ca(1)−O(18)	2.331(4)
Mn(1)−O(5)−N(3)−Mn(4)	154.4	Mn(1)−O(5)−Ca(1)	122.1(2)
Mn(2)−O(22)−N(5)−Mn(1)	164.9	Mn(2)−O(1)−Ca(1)	120.2(2)
Mn(3)−O(2)−N(4)−Mn(2)	163.5	Mn(3)−O(2)−Ca(1)	120.1(2)

dx.doi.org/10.1021/ic502492x | Inorg. Chem. 2015, 54, 2137−2151

Table 2. continued

		$3{\cdot}2CH_2Cl_2$	
Mn(4)−O(6)−N(1)−Mn(3)	173.5	Mn(4)−O(6)−Ca(1)	119.0(2)
		$4{\cdot}5CH_2Cl_2$	
Mn(1)···Mn(2)	4.589(2)	Mn(2)···Mn(4)	6.593(4)
Mn(2)···Mn(3)	4.599(2)	Mn(1)···Ca(1)	3.729(1)
Mn(3)···Mn(4)	4.645(3)	Mn(2)···Ca(1)	3.721(1)
Mn(4)···Mn(1)	4.595(2)	Mn(3)···Ca(1)	3.804(1)
Mn(1)···Mn(3)	6.426(3)	Mn(4)···Ca(1)	3.773(1)
Mn(1)−O(1)	1.872(3)	Mn(3)−O(9)	1.889(3)
Mn(1)−O(6)	1.846(3)	Mn(3)−O(11)	2.165(3)
Mn(1)−O(13)	2.070(3)	Mn(3)−O(16)	1.975(3)
Mn(1)−O(20)	1.931(3)	Mn(3)−O(17)	1.865(3)
Mn(1)−N(1)	1.956(3)	Mn(3)−N(3)	1.975(3)
Mn(2)−O(2)	1.881(3)	Mn(4)−O(3)	1.890(3)
Mn(2)−O(15)	2.073(3)	Mn(4)−O(4)	1.871(3)
Mn(2)−O(18)	1.931(3)	Mn(4)−O(5)	1.950(3)
Mn(2)−O(19)	1.863(3)	Mn(4)−O(7)	2.118(3)
Mn(2)−N(4)	1.959(4)	Mn(4)−N(2)	1.975(4)
Ca(1)−O(1)	2.422(3)	Ca(1)−O(9)	2.495(3)
Ca(1)−O(2)	2.423(3)	Ca(1)−O(10)	2.335(3)
Ca(1)−O(4)	2.448(3)	Ca(1)−O(12)	2.389(4)
Ca(1)−O(8)	2.421(3)	Ca(1)−O(14)	2.375(3)
Mn(1)−O(1)−N(4)−Mn(2)	171.5	Mn(1)−O(1)−Ca(1)	120.0(1)
Mn(2)−O(2)−N(3)−Mn(3)	165.3	Mn(2)−O(2)−Ca(1)	119.1(2)
Mn(3)−O(9)−N(2)−Mn(4)	171.4	Mn(3)−O(9)−Ca(1)	119.7(1)
Mn(4)−O(4)−N(1)−Mn(1)	169.2	Mn(4)−O(4)−Ca(1)	121.2(1)

[a]Symmetry code: ′ = 1 − *x*, −*y*, −*z*.

$P2_1/n$ space groups, respectively. Selected interatomic distances and angles for complexes **1**, **2**, and **4** are listed in Table 2.

The core of **4** consists of four Mn^{III} and one Ca^{II} atoms arranged in a slightly distorted square pyramidal topology (Figure 2, left), with the Ca^{II} atom occupying the apical position and the Mn^{III} atoms forming the square base. The Mn···Mn···Mn angles are spanning the range of 88.1−91.8°, deviating only slightly from the ideal 90°, and the Mn···Ca···Mn angles of the four triangular faces lie within the 75.3−76.1° range. The Mn^{III} atoms form a near-planar square, with each of the edges bridged by a diatomic oximate group from a shi^{3-} ligand, thus giving Mn···Mn separations of 4.589(1)−4.645(1) Å. The almost perfectly planar Mn_4 unit is clearly due to the large Mn−O−N−Mn torsion angles of 171.5° (Mn1−O1−N4−Mn2), 165.3° (Mn2−O2−N3−Mn3), 171.3° (Mn3−O9−N2−Mn4), and 169.2° (Mn4−O4−N1−Mn1), very close to the ideal linearity of 180°. The linkage between the basal Mn^{III} atoms and the apical Ca^{II} atom is provided by the oximate O atoms of shi^{3-} ligands and the four $\eta^1{:}\eta^1{:}\mu$ bidentate bridging pyrene carboxylate ($L3^-$) groups. The Mn···Ca separations [3.773(1), 3.804(1), 3.729(1), and 3.721(1) Å] in the square pyramid of **4** are in close proximity with conclusions from Ca EXAFS studies on the $\{Mn_4Ca\}$ extended cubane of OEC (approximately 3.4 Å).[40] Differences between the Mn···Ca separations of **4** and those of OEC are to be expected given the different core topologies, greater distance uncertainties in the crystal structure of a large PSII multicomponent assembly, structural perturbations caused by the polypeptide environment, and the fact that some of the Mn atoms of OEC in the PSII crystal structure will be at a higher oxidation state (i.e., Mn^{IV}), leading to shorter bond distances on average.[13,41]

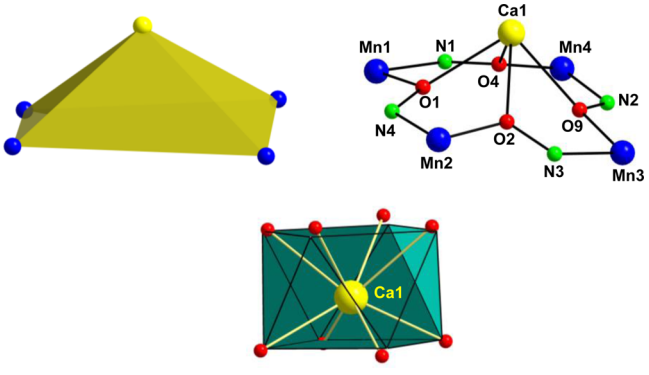

Figure 2. Labeled representations of the $\{Mn_4Ca\}$ square pyramidal topology (top, left) and the complete $[Mn_4Ca(\mu\text{-}NO)_4]^{10+}$ core of representative complex **4** (top, right). Square antiprismatic coordination geometry of Ca^{II} atom in **4**; the points connected by the black lines define the vertices of the ideal polyhedron. Color scheme as in Figure 1.

Ligation around each Mn^{III} atom is completed by the alkoxido and phenoxido O atoms from shi^{3-} groups; the latter are thus $\eta^1{:}\eta^1{:}\eta^1{:}\eta^2{:}\mu_3$. The complex therefore contains an overall $[Mn_4Ca(\mu\text{-}NO)_4]^{10+}$ core (Figure 2, right), which can also be described as a $[12\text{-}MC_{Mn(III)N(shi)}\text{-}4]$ metallacrown[42] surrounding a Ca^{II} atom. The latter lies 1.873 Å out of the Mn_4 plane. All Ca−O bonds are in the range of 2.335(3)−2.495(3) Å. All Mn^{III} atoms in **1**, **2**, and **4** are five-coordinate with almost perfect square pyramidal geometries. This is confirmed by analysis of the shape-determining bond angles using the approach of Reedijk and Addison,[43] which yields an average value for the trigonality index, τ, of 0.04 for the four metal ions, where τ is 0 and 1 for perfect square pyramidal and trigonal bipyramidal geometries, respectively. The Mn oxidation states

dx.doi.org/10.1021/ic502492x | Inorg. Chem. 2015, 54, 2137−2151

were established by charge balance considerations, metric parameters, and bond valence sum calculations (BVS, Table 3).[44] In all the compounds, the Ca^{II} atom is eight-coordinate in a CaO_8 environment possessing square antiprismatic geometry. That was confirmed by the continuous shape measure (CShM) approach, which essentially allows one to numerically evaluate by how much a particular structure deviates from an ideal shape.[45] The best fit was obtained for the square antiprism (Figure 2, bottom) with CShM value of 0.77. Values of CShM between 0.1 and 3 usually correspond to a not negligible but still small distortion from ideal geometry.[46]

Table 3. BVS Calculations[a] for Mn Atoms in 1−4

complex	atom	Mn^{II}	Mn^{III}	Mn^{IV}
1	Mn1	3.27	3.04	3.12
	Mn2	3.35	3.11	3.20
2	Mn1	3.30	3.05	3.14
	Mn2	3.24	3.00	3.09
	Mn3	3.18	2.95	3.03
	Mn4	3.20	2.96	3.05
3	Mn1	3.21	2.97	3.06
	Mn2	3.27	3.03	2.86
	Mn3	3.25	3.01	3.10
	Mn4	3.28	3.03	3.13
4	Mn1	3.38	3.13	3.22
	Mn2	3.31	3.07	3.16
	Mn3	3.10	2.87	2.95
	Mn4	3.17	2.94	3.02

[a]The underlined value is the one closest to the charge for which it was calculated. The oxidation state is the nearest whole number to the underlined value.

Complex $(NHEt_3)_5[Mn_4Ca(L2)_4(shi)_4(shiH_2)_2](ClO_4)$ (**3**) has a very similar structure (Figure 3) to that of **2**, the only significant difference being the terminal (η^1) coordination of two singly deprotonated $shiH_2^-$ ligands on two Mn^{III} atoms (Mn2 and Mn4). As a result, Mn2 and Mn4 exhibit a near-octahedral geometry that takes the form of an axially elongated Jahn−Teller (JT) distortion, as expected for a high-spin d^4 ion in this geometry. The JT axes in both Mn sites involve the anthracene carboxylate and $shiH_2^-$ phenoxido O atoms. The noncoordinated N and the oximato and alkoxido O atoms of $shiH_2^-$ are strongly H-bonded to two Et_3NH^+ countercations.

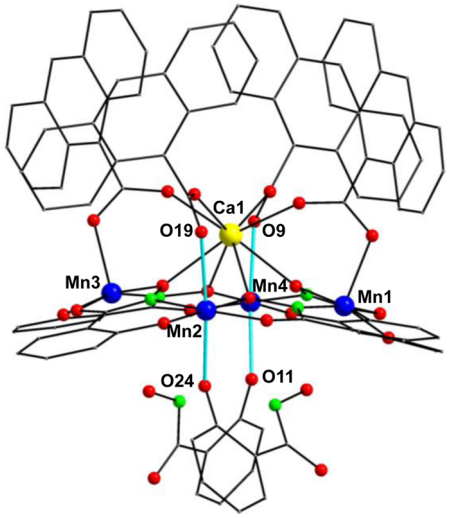

Figure 3. Partially labeled representation of the structure of the anion present in complex **3**, with the cyan thick bonds emphasizing the JT axes of six-coordinate Mn^{III} atoms. H atoms are omitted for clarity. Color scheme as in Figure 1.

From a supramolecular viewpoint, all reported compounds **1**−**4** show similar intramolecular H-bonding interactions that include the Et_3NH^+ cations as donors and the O atoms of carboxylate ligands as acceptors. The pyrene analogue **4** shows two sets of intramolecular $\pi-\pi$ stacking interactions between adjacent centroids, as defined by C9−C24 (centroid A)/C30−C45 (centroid B), and C47−C62 (centroid C)/C64−C79 (centroid D); their distances are centroid A··· centroid B = 3.807 Å and centroid C··· centroid D = 3.835 Å (Supporting Information, Figure S1). Finally, the crystal structures of all complexes exhibit intermolecular interactions that involve the aromatic rings of the ligands and H-bonding interactions between the countercations, lattice solvate molecules, and coordinated ligands. The shortest, intermolecular Mn···Mn distances between neighboring cluster compounds are 6.461 (for **1**), 8.445 (for **2**), 8.789 (for **3**), and 6.881 Å (for **4**).

It is quite intriguing that Mn−Ca heterometallic chemistry has not been so extensively developed as Mn-3d′ and Mn-4f mixed-metal chemistry although it has attracted the interest of many inorganic synthetic chemists during the last three decades or so. Complexes **1**−**4** join only a handful of previous Mn−Ca compounds,[11−13] and together with $(NHEt_3)_2[Mn^{III}_4Ca(O_2CPh)_4(shi)_4]$,[18] these are the only structurally characterized species with a 4:1 Mn/Ca ratio and all Mn atoms in +3 oxidation state.

Electronic Spectra and Electrospray Ionization Mass Spectrometry (ESI-MS). UV−vis and ESI-MS studies were performed to probe the structural integrity of **1**−**4** in solution and elucidate any possible photophysical properties. The electronic absorption spectra of isostructural complexes **1**, **2**, and **4** were recorded in MeCN solutions of concentrations ≈ 10^{-5} M (Figure 4). All three compounds show the characteristic bands (shoulders and/or sharp peaks) of naphthalene, anthracene, and pyrene functional groups slightly shifted to higher wavenumbers, consistent with coordination of the fluorescence carboxylate ligands to the metal centers.[47] The high-intensity absorption bands in the 240−350 nm region are

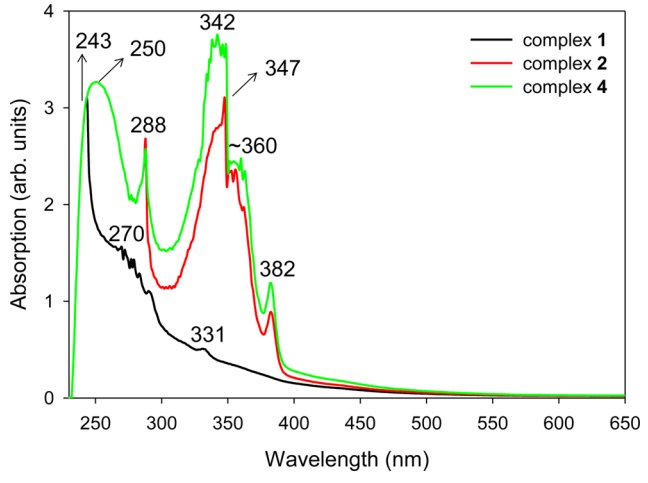

Figure 4. Absorption spectra of complexes **1**, **2**, and **4** in MeCN (~10^{-5} M).

dx.doi.org/10.1021/ic502492x | Inorg. Chem. 2015, 54, 2137−2151

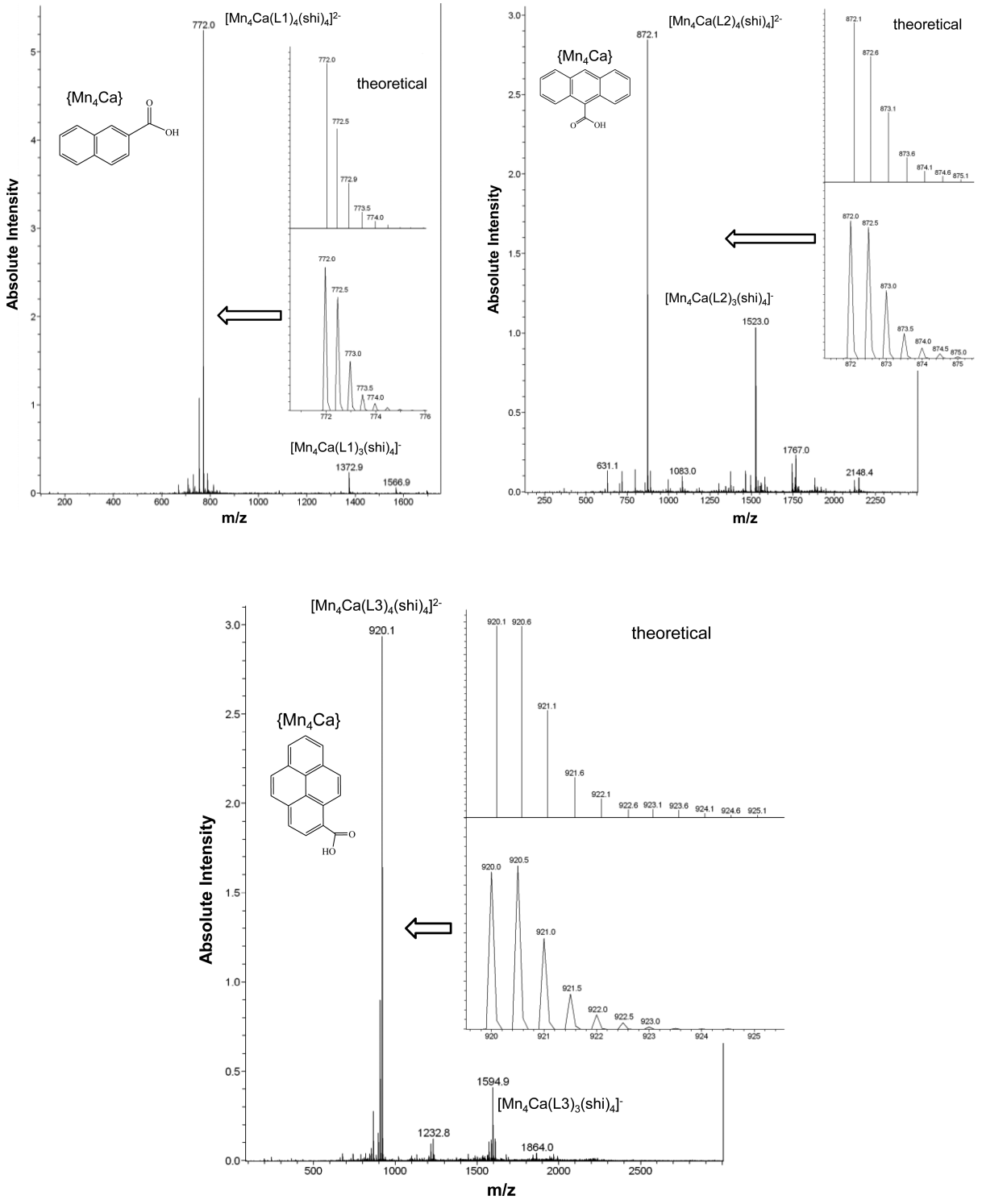

Figure 5. Negative ion ES mass spectra of **1** (top, left), **2** (top, right), and **4** (bottom) in MeCN. Insets illustrate the zoomed region around the predominant $[Mn_4Ca(LX)_4(shi)_4]^{2-}$ dianions (X = 1−3) and the corresponding, theoretically calculated, isotopic distributions.

assigned to $\pi-\pi^*$ transitions within the aromatic organic ligands, while the less-intense bands at ∼380 nm are possibly due to ligand-to-metal charge transfer effects.[48] Note that the absorption bands of neutral salicylhydroxamic acid (218, 236, and 300 nm) appear to overlap with the bands of polyaromatic carboxylate ligands upon coordination with the metal centers. Hence, the conclusions from the UV−vis studies were very promising that compounds **1**, **2**, and **4** retain their solid-state $\{Mn_4Ca\}$ structures in solution, and confirmation was sought by electrospray ionization (ESI) mass spectrometry (MS).

Negative (−) ion ES-MS studies were conducted to investigate the stability of complexes **1**, **2**, and **4** in the aprotic MeCN solvent. Unfortunately, due to the paramagnetic nature of **1**−**4**, solution NMR spectroscopy could not provide any useful structural information. In contrast, ESI-MS is a soft technique that (i) allows the detection of multiply charged ions, (ii) does not alter the connectivity of the compounds (through

dx.doi.org/10.1021/ic502492x | Inorg. Chem. 2015, 54, 2137−2151

disassembly and reassembly processes), and (iii) causes very little fragmentation.[49] Although very rare in volatile transition metal cluster chemistry, all three described compounds proved to preserve their core structures in solution with high-intensity ion signals corresponding to the sole presence of $\{Mn_4Ca\}$ cores without major fragment ions. For complexes **1**, **2**, and **4**, the strong intensity peaks at 772, 872, and 920 m/z nicely reproduce the doubly charged $[Mn_4Ca(L1)_4(shi)_4]^{2-}$, $[Mn_4Ca(L2)_4(shi)_4]^{2-}$, and $[Mn_4Ca(L3)_4(shi)_4]^{2-}$ species, respectively (Figure 5). In support of these assignments is the excellent match observed between the acquired isotopic patterns of $[Mn_4Ca(LX)_4(shi)_4]^{2-}$ ions (X = 1−3) and the theoretically calculated distributions (Figure 5, insets), allowing us to confirm the structural integrity of **1**, **2**, and **4** in MeCN. The very low intensity peaks at 1373, 1523, and 1595 m/z can be assigned to the least abundant, singly anionic fragments $[Mn_4Ca(L1)_3(shi)_4]^-$, $[Mn_4Ca(L2)_3(shi)_4]^-$, and $[Mn_4Ca(L3)_3(shi)_4]^-$, respectively, which correspond to the reported $\{Mn_4Ca\}$ core structures with the dissociation of one carboxylate ligand.

Electrochemistry. The redox activity of electrochemically prominent metal complexes can be assessed by cyclic voltammetry. This technique is of significant importance in both molecular magnetism and bioinorganic chemistry. For example, in the molecular magnetism arena, electrochemical studies of various $[Mn^{III}_8Mn^{IV}_4O_{12}(O_2CR)_{16}(H_2O)_4]$ compounds have revealed a rich redox chemistry involving several quasi-reversible oxidation and reduction processes.[50] Four different oxidation levels of this family of clusters have been isolated, and the corresponding 1-, 2-, 3-, and 4-electron reduced species were characterized in the solid-state and demonstrated their distinct single-molecule magnetism properties compared to the parent $[Mn_{12}]$ complex.[51] In the bioinorganic and biomimetic fields related to PSII, it is now well-documented that Mn ions within OEC show a high degree of redox and chemical versatility, while the protein residues and coordination environment are both critical for modulating the redox potentials and providing pathways for electron- and proton-transfer effects.[52] For example, in the S_0 state of OEC cycle, EPR, XANES, and ENDOR studies have proposed two different formal oxidation states, II/III/IV/IV and III/III/III/IV, for the Mn atoms.[53]

Toward that end, the electrochemical properties of complexes **1**, **2**, and **4** were studied in MeCN and all showed that they exhibit very similar redox processes. The cyclic voltammogram (CV) of complex **1** is shown in Figure 6 (top). It displays a well-defined reversible oxidation at ∼0.43 V and an irreversible reduction that corresponds to the broad peak at −0.47 V. The CV spectra of the anthracene analogue **2** (Figure 6, middle) and pyrene-substituted **4** (Figure 6, bottom) show very similar patterns comprising well-defined reversible oxidations at ∼0.44 and ∼0.42 V, and irreversible reductions associated with the appearance of weak and broad peaks at −0.78 and −0.79 V, respectively. For the reversible oxidation couple of all three studied compounds, the forward and reverse waves are well-formed with a peak separation of 70 (**1**), 190 (**2**), and 100 (**4**) mV comparable to that of ferrocene under the same conditions; this is indicative of a one-electron process.[54] In summary, all complexes exhibited a similar oxidation, but the reduction waves seemed to be slightly different. Such small discrepancies most likely result from the different nature of the carboxylate ligand. It is known that in isostructural, high oxidation state Mn complexes the identity, basicity, and steric

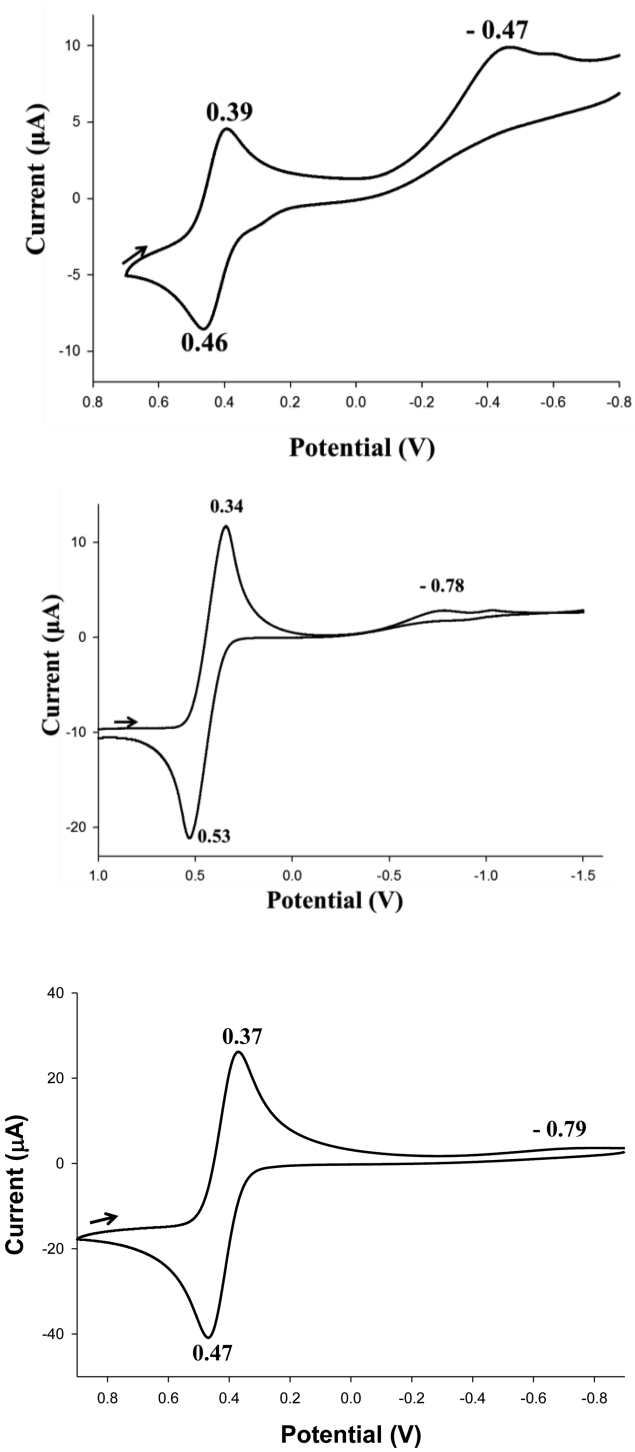

Figure 6. Cyclic voltammograms at 100 mV s^{-1} for complexes **1** (top), **2** (middle), and **4** (bottom) in MeCN containing 0.1 M $N^nBu_4PF_6$ as supporting electrolyte. The indicated potentials are vs Fc/Fc^+.

and electronic properties of the carboxylate ligands affect the sensitivity of metal ions' redox potentials.[55] The electrochemical results may be illustrated as $[Mn_4Ca]^+ \leftrightarrow [Mn_4Ca] \rightarrow [Mn_4Ca]^-$. Synthetic efforts to isolate and structurally characterize the monocation are objectives for future research efforts to address and accomplish.

Photophysical Studies. The pronounced ability of complexes **1**−**4** to retain their structures in solution prompted us to further investigate their optical activity at room

dx.doi.org/10.1021/ic502492x | Inorg. Chem. 2015, 54, 2137−2151

temperature conditions. We have thus decided to perform excitation/emission studies in MeCN solutions of **1**, **2**, and **4** at concentrations $\approx 10^{-5}$ M. Very recently, Chia and Tay overviewed the difficulties in obtaining emissions from transition metal complexes, usually produced from triplet excited states, as a result of the fast intersystem crossing facilitated by the strong spin−orbit coupling.[56] It is also known that quenching of the emission intensity due to paramagnetic effects is a common feature in 3d-metal complexes.[57] To tackle this problem, the use of organic bridging groups with emission dyes seems to be a promising route.

The fluorescence behaviors of the free, uncoordinated $shaH_2$ and LX-H (X = 1−3) ligands are well-known in both solid-state and solution. For instance, and with relevance to our studies, $shaH_2$ in MeCN shows a maximum emission at 450 nm upon maximum excitation at 346 nm.[58] Complex **1** shows an intense emission at 396 nm upon excitation at the maximum observed at 300 nm (Figure 7, top); the location of the emission peak is at the same area where naphthalene emits but slightly shifted, indicative of charge transfer from the ligands to the cluster core.[59] A light brown solution of complex **2** in MeCN also shows a very strong "blue"-shifted emission upon excitation at the UV region, with the three emission peaks at 391, 410, and 433 nm attributed to the characteristic peaks of anthracene chromophore (Figure 7, middle).[21,60] Interestingly, complex **4** displays two sharp emission peaks at 392 and 408 nm, upon UV excitation at 380 nm, which are characteristic of the corresponding monomer and excimer emissions of the pyrene unit.[22,61] The formation of a pyrene excimer requires an excited molecule to come in contact with another molecule in its ground state within the excited-state lifetime. For this to occur, the pyrene units must be well-isolated from each other such that excitation is localized on one of the molecules, and then diffusion of the molecule will allow for an encounter between an excited pyrene and a ground-state one. In such an ideal case, the fluorescence emission of pyrene excimers appears as a broad, structureless band located at 470−500 nm.[62] In complex **4** the excimer peak has been blue-shifted, and this is likely due to its coordination with the metal centers and the presence of significant intramolecular $\pi-\pi^*$ interactions, which bring the pyrene units into close contacts.

Solid-State Magnetic Susceptibility Studies. Variable-temperature magnetic susceptibility measurements were performed on powdered polycrystalline samples of complexes **1**, **3**, and **4**, restrained in eicosane to prevent torquing, in a 1 kG (0.1 T) field and in the 5.0−300 K range. The data are shown as $\chi_M T$ versus T plots in Figure 8. The isostructural complexes **1** and **4** exhibited similar magnetic behavior (vide infra), and we have thus decided to perform magnetic studies on the slightly different complex **3** instead of **2**; however, the magnetic response was again similar to that of **1** and **4**. The $\chi_M T$ product for all three compounds steadily decreases from 12.09 (**1**), 12.19 (**3**), and 9.53 (**4**) cm^3 K mol^{-1} at 300 K to 1.32 (**1**), 1.35 (**3**), and 0.62 (**4**) cm^3 K mol^{-1} at 5.0 K. The 300 K values are close to or less than (in case of the pyrene analogue **4**) the spin-only (g = 2) value of 12 cm^3 K mol^{-1} for four noninteracting Mn^{III} ions, similar to the $\chi_M T$ value of the previously reported $[Mn_4Ca(O_2CPh)_4(shi)_4]^{2-}$.[18] The shape of the $\chi_M T$ versus T curves clearly indicates the presence of predominant antiferromagnetic exchange interactions between the four Mn^{III} atoms and a resulting S = 0 ground state for each of the reported compounds.

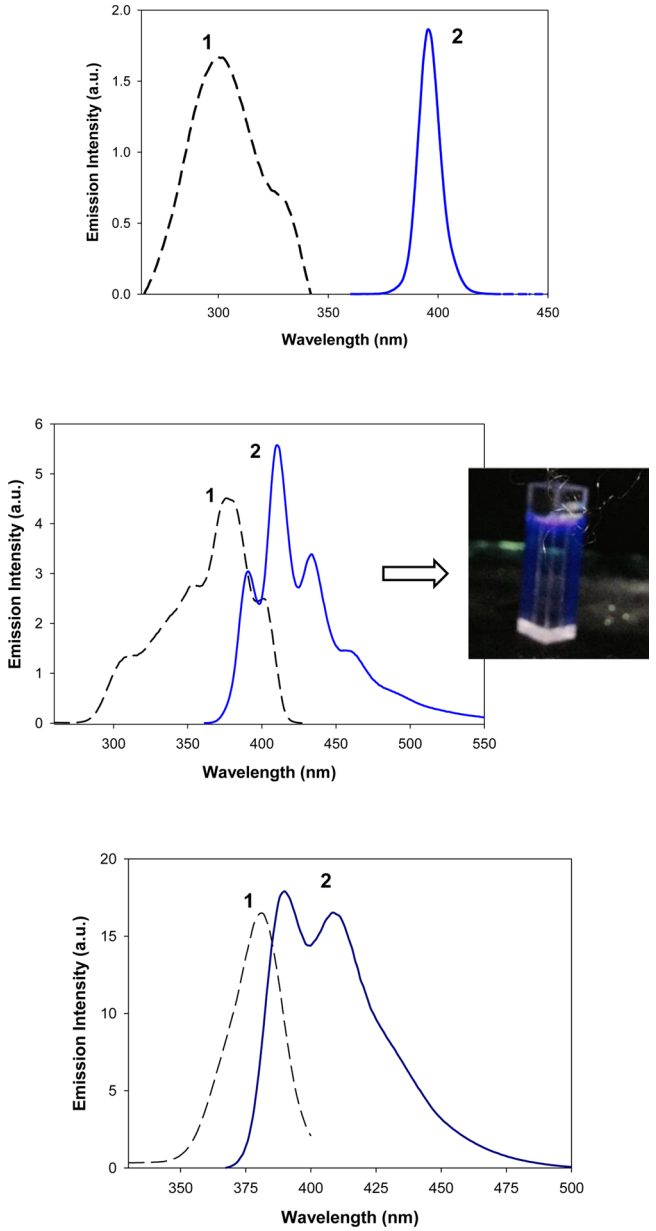

Figure 7. Excitation (1) and emission (2) spectra of complexes **1** (top), **2** (middle), and **4** (bottom) in MeCN. The inset highlights a photograph of complex **2** under a UV lamp.

To determine the individual pairwise exchange parameters J_{ij} between Mn_iMn_j pairs within the magnetic cores, the $\chi_M T$ versus T data for complexes **1**, **3**, and **4** were fit to the theoretical expression for a Mn_4^{III} square (inset of Figure 8, top) using the isotropic Heisenberg spin Hamiltonian given by eq 3.

$$\mathcal{H} = -2J(\hat{S}_1\cdot\hat{S}_2 + \hat{S}_2\cdot\hat{S}_3 + \hat{S}_3\cdot\hat{S}_4 + \hat{S}_1\cdot\hat{S}_4) \quad (3)$$

In light of the very similar Mn−N−O−Mn torsion angles and Mn···Mn separations within the Mn_4 square, all interactions between neighboring Mn^{III} atoms were considered as equivalent (1-J model). The fit parameters were thus J and g. A temperature-independent paramagnetism (TIP) term was also included in all cases. Data below 30 K were omitted to avoid effects from Zeeman interactions, magnetic anisotropy (zero-field splitting, D), and crystal structure disorders; these are all factors that are not included in the above model.[22] Good

dx.doi.org/10.1021/ic502492x | Inorg. Chem. 2015, 54, 2137−2151

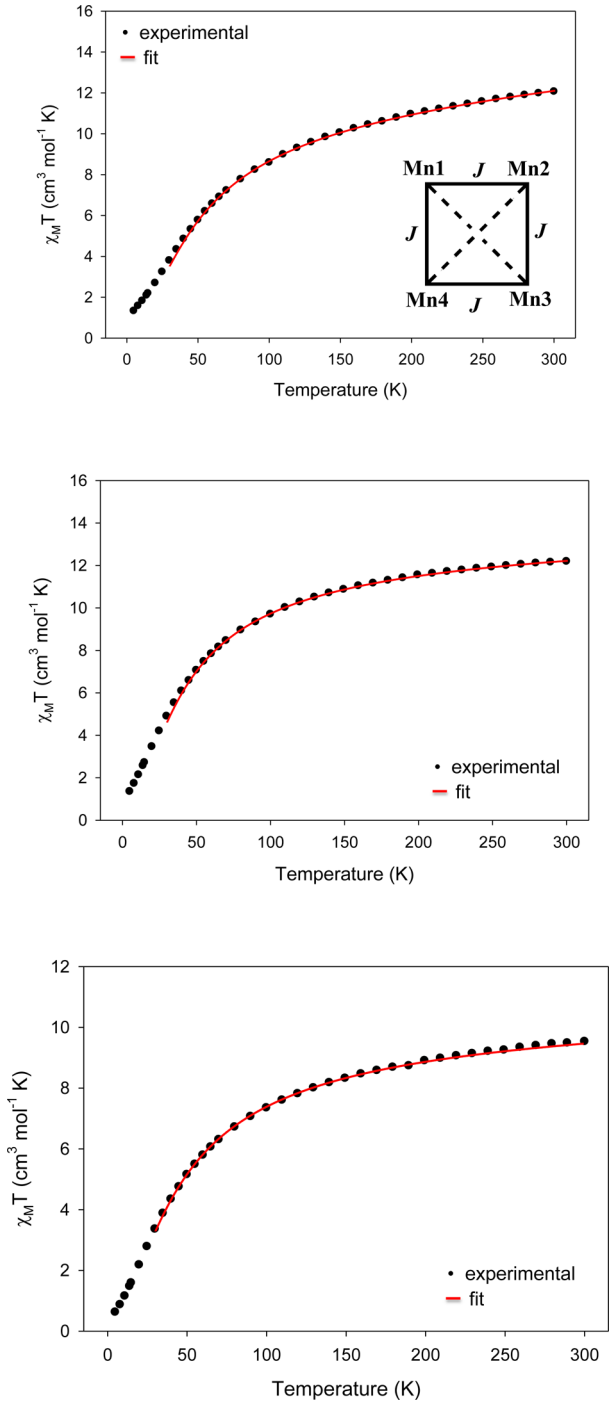

Figure 8. $\chi_M T$ vs T plots for **1** (top), **3** (middle), and **4** (bottom) at 0.1 T direct current field. The red solid line is the fit of the corresponding data; see the text for the fit parameters. (inset) 1-J coupling scheme used for all complexes.

fits were obtained for all three complexes, and these are shown as solid lines in Figure 8. The best-fit parameters were: J = −3.17(4) cm^{-1}, g = 1.97(1), and TIP = 6×10^{-3} cm^3 mol^{-1} for **1**; J = −2.73(2) cm^{-1}, g = 2.10(4), and TIP = 10^{-3} cm^3 mol^{-1} for **3**; and J = −2.98(2) cm^{-1}, g = 1.86(2), and TIP = 8×10^{-4} cm^3 mol^{-1} for **4**. The fits of the data indicate S = 0 ground states and S = 1 first excited states lying 6.34, 5.46, and 5.96 cm^{-1} higher in energy, respectively. Attempts to include a D term into the fitting process, using the program PHI,[63] failed to give us a better low-temperature fit. Fits of the data to a 2-J model, assuming that the next-nearest neighbor interactions across the diagonal Mn sites are not zero, gave results of comparable quality (Supporting Information, Figure S2). These, however, could lead to overparameterization problems, and therefore the long $Mn^{III}\cdots Mn^{III}$ exchange interactions can be ignored. Finally, none of the magnetically studied complexes showed peak maxima in the $\chi_M T$ versus T plots. The antiferromagnetic interactions in all compounds are as expected for systems coupled solely through oximate bridges with very large M−N−O−M (M = 3d-metal ion) torsion angles (>160°).[64]

Relevance of Complexes 1−4 to Low-Oxidation States of OEC: A Qualitative Approach. In the absence of advanced XAS, EXAFS, and ENDOR studies, which would shine more light into the similarities of **1**−**4** with OEC, we provide instead a qualitative and brief discussion of the relevance of reported compounds to some species of the native enzyme. Complexes **1**−**4** have the same Mn_4Ca content and carboxylate ligation as the OEC. We recognize that within the structures of all complexes the average Mn···Mn (between closest neighbors) and Mn···Ca separations are ∼4.6 and ∼3.7 Å, respectively, significantly longer than the corresponding values of 2.7−3.3 and ∼3.4 Å for the OEC in PSII. However, the structures of the reported compounds may be relevant to the OEC in other ways. On the basis of the S_1 Kok state of the OEC being at the $2Mn^{III},2Mn^{IV}$ oxidation level, the Mn^{III}_4 level of **1**−**4** would place them at the S_{-1} state. Hydrazine (N_2H_4), hydroxylamine (NH_2OH), and nitric oxide are known to be able to reduce the OEC to S_{-1}, S_{-2}, and even S_{-3} states.[65] These are not involved in the water oxidation catalytic cycle but may be related to intermediates during the in vivo assembly of the OEC. Assuming these involve Mn-based reductions, then they would be at the $4Mn^{III}$, $Mn^{II},3Mn^{III}$ and $2Mn^{II},2Mn^{III}$ levels, respectively; an EPR signal assignable to a $Mn^{II}Mn^{III}$ subunit has been detected for S_{-2}.[66] It is thus possible that the structures of complexes **1**−**4** may be of more relevance to these lower oxidation state forms of the OEC that will have a lower preference for oxido bridges than to the higher oxidation states that have a cubane structure and are involved in the catalytic cycle. Along these lines, the similarity between the oximato N−O bridging unit of shi^{3-} within **1**−**4** and the M−N−O−M unit seen in hydroxylamine-bridged metal complexes[67] is intriguing and suggests that **1**−**4** may be providing insights into the kind of subunits that might be generated on reduction of the OEC with NH_2OH.

CONCLUSIONS

To summarize, we have shown that salicylhydroxime scaffold can provide the means of obtaining new heterometallic Mn/Ca clusters with the same Mn_4Ca stoichiometry as the OEC and the four Mn ions in a moderate 3+ oxidation level. In addition, the incorporation of fluorescent carboxylate groups as supporting ligands about the paramagnetic Mn_4Ca core has also enabled us to gain access to some interesting photophysical properties such as blue-shifted emissions at room temperature. The reported compounds are also very rare examples of metal clusters that retain their solid-state structures in solution, as accurately confirmed by ESI-MS. This is most likely due to the pronounced stability of the Mn_4Ca metallacrown core induced by the four donor atoms of the salicylhydroximate ligand.

It must be admitted that the core of **1**−**4** is different from the distorted-cubane core found in the native OEC but may be relevant to lower oxidation level species that are intermediates

dx.doi.org/10.1021/ic502492x | Inorg. Chem. 2015, 54, 2137−2151

during assembly of the OEC in vivo or to those generated by treatment of the OEC with strong reducing agents. By taking into account the well-defined reversible oxidation observed in all studied $Mn_4^{III}Ca$ compounds, we are now seeking methods to isolate the one-electron oxidized species that would facilitate the stabilization of O^{2-} groups and consequently the formation of an oxido-bridged metal core, structurally closer to that seen in the OEC and more susceptible in resembling the S_0 state of the Kok cycle.

■ ASSOCIATED CONTENT

Supporting Information

Crystallographic data for all reported compounds in CIF format, supramolecular $\pi-\pi$ stacking interactions, and $\chi_M T$ versus T plots. This material is available free of charge via the Internet at http://pubs.acs.org. Crystallographic data (excluding structure factors) for the structures reported in this work have been deposited to the Cambridge Crystallographic Data Centre (CCDC) as supplementary publication numbers CCDC-1027595 (**1**), 1027596 (**2**·$4CH_2Cl_2$), 1027597 (**3**·$2CH_2Cl_2$), and 1027598 (**4**·$5CH_2Cl_2$). Copies of these data can be obtained free of charge on application to CCDC, 12 Union Road, Cambridge CB2 2EZ, U.K.; FAX: (+44) 1223 336033, or online via www.ccdc.cam.ac.uk/data_request/cif or by emailing data_request@ccdc.cam.ac.uk.

■ AUTHOR INFORMATION

Corresponding Author

*E-mail: tstamatatos@brocku.ca.

Notes

The authors declare no competing financial interest.

■ ACKNOWLEDGMENTS

We thank NSERC Discovery Grant, Brock University, and CFI (to T.C.S), and the National Science Foundation (DMR-1213030 to G.C.) for funding. L.C.-S. acknowledges financial support from the Fundação para a Ciência e a Tecnologia (FCT, Portugal) under the strategic project Pest-C/EQB/LA0006/2013 (to REQUIMTE), and the European Synchrotron Radiation Facility (Grenoble, France) for granting access time to the Swiss–Norwegian BM01a beamline under the research proposals CH-3613 and CH-3849. We also thank Dr. T. Jones for the collection of the ESI-MS data.

■ REFERENCES

(1) (a) Williamson, A.; Conlan, B.; Hillier, W.; Wydrzynski, T. *Photosynth. Res.* **2011**, *107*, 71–86. (b) Des Marais, D. J. *Science* **2000**, *289*, 1703–1705. (c) Allen, J. F.; Martin, W. *Nature* **2007**, *445*, 610–612.

(2) (a) Yano, J.; Yachandra, V. *Chem. Rev.* **2014**, *114*, 4175–4205. (b) Yano, J.; Kern, J.; Sauer, K.; Latimer, M. J.; Pushkar, Y.; Biesiadka, J.; Loll, B.; Saenger, W.; Messinger, J.; Zouni, A.; Yachandra, V. K. *Science* **2006**, *314*, 821–825.

(3) Kok, B.; Forbush, B.; McGloin, M. *Photochem. Photobiol.* **1970**, *11*, 457–475.

(4) (a) Joliot, P. *Biochim. Biophys. Acta* **1965**, *102*, 116–134. (b) Haumann, M.; Liebisch, P.; Müller, C.; Barra, M.; Grabolle, M.; Dau, H. *Science* **2005**, *310*, 1019–1021.

(5) Kolling, D. R. J.; Cox, N.; Ananyev, G. M.; Pace, R. J.; Dismukes, G. C. *Biophys. J.* **2012**, *103*, 313–322.

(6) (a) Visser, H.; Anxolabehere-Mallart, E.; Bergmann, U.; Glatzel, P.; Robblee, J. H.; Cramer, S. P.; Girerd, J.-J.; Sauer, K.; Klein, M. P.; Yachandra, V. K. *J. Am. Chem. Soc.* **2001**, *123*, 7031–7039. (b) McEvoy, J. P.; Brudvig, G. W. *Chem. Rev.* **2006**, *106*, 4455–4483. (c) Pecoraro, V. L.; Baldwin, M. J.; Caudle, M. T.; Hsieh, W. Y.; Law, N. A. *Pure Appl. Chem.* **1998**, *70*, 925–929. (d) Glatzel, P.; Schroeder, H.; Pushkar, Y.; Boron, T.; Mukherjee, S.; Christou, G.; Pecoraro, V. L.; Messinger, J.; Yachandra, V. K.; Bergmann; Yano, J. *Inorg. Chem.* **2013**, *52*, 5642–5644. (e) Meelich, K.; Zaleski, C. M.; Pecoraro, V. L. *Philos. Trans. R. Soc., B* **2008**, *363*, 1271–1281.

(7) Loll, B.; Kern, J.; Saenger, W.; Zouni, A.; Biesiadka, J. *Nature* **2005**, *438*, 1040–1044.

(8) Umena, Y.; Kawakami, K.; Shen, J.-R.; Kamiya, N. *Nature* **2011**, *473*, 55–60.

(9) (a) Miller, A. F.; Brudvig, G. W. *Biochemistry* **1990**, *29*, 1385–1392. (b) Burnap, R. L. *Phys. Chem. Chem. Phys.* **2004**, *6*, 4803–4809.

(10) For recent reviews in polynuclear Mn clusters, see: (a) Kostakis, G. E.; Blatov, V. E.; Proserpio, D. M. *Dalton Trans.* **2012**, *41*, 4634–4640. (b) Aromí, G.; Brechin, E. K. *Struct. Bonding (Berlin)* **2006**, *122*, 1–67. (c) Tasiopoulos, A. J.; Perlepes, S. P. *Dalton Trans.* **2008**, 5537–5555.

(11) (a) Mishra, A.; Wernsdorfer, W.; Abboud, K. A.; Christou, G. *Chem. Commun.* **2005**, 54–56. (b) Gorun, S. M.; Stibrany, R. T.; Lillo, A. *Inorg. Chem.* **1998**, *37*, 836–837. (c) Hewitt, I. J.; Tang, J. K.; Madhu, N. T.; Clérac, R.; Buth, G.; Anson, C. E.; Powell, A. K. *Chem. Commun.* **2006**, 2650–2652. (d) Nayak, S.; Nayek, H. P.; Dehnen, S.; Powell, A. K.; Reedijk, J. *Dalton Trans.* **2011**, *40*, 2699–2702. (e) Kotzabasaki, V.; Siczek, M.; Lis, T.; Milios, C. J. *Inorg. Chem. Commun.* **2011**, *14*, 213–216. (f) Jerzykiewicz, L. B.; Utko, J.; Duczmal, M.; Sobota, P. *Dalton Trans.* **2007**, 825–826.

(12) (a) Kanady, J. S.; Tsui, E. Y.; Day, M. W.; Agapie, Th. *Science* **2011**, *333*, 733–736. (b) Tsui, E. Y.; Tran, R.; Yano, J.; Agapie, T. *Nat. Chem.* **2013**, *5*, 293–299.

(13) Mukherjee, S.; Stull, J. A.; Yano, J.; Stamatatos, T. C.; Pringouri, K.; Stich, T. A.; Abboud, K. A.; Britt, R. D.; Yachandra, V. K.; Christou, G. *Proc. Natl. Acad. Sci. U. S. A.* **2012**, *109*, 2257–2262.

(14) (a) Campbell, K. A.; Force, D. A.; Nixon, P. J.; Dole, F.; Diner, B. A.; Britt, R. D. *J. Am. Chem. Soc.* **2000**, *122*, 3754–3761. (b) Dasgupta, J.; Ananyev, G. M.; Dismukes, G. C. *Coord. Chem. Rev.* **2008**, *252*, 347–360.

(15) (a) Mukhopadhyay, S.; Mandal, S. K.; Bhaduri, S.; Armstrong, W. H. *Chem. Rev.* **2004**, *104*, 3981–4026. (b) Brudvig, G. W.; Beck, W. F. In *Manganese Redox Enzymes;* Pecoraro, V. L., Ed.; VCH Publishers, Inc.: New York, 1992; pp 119–140.

(16) (a) Schansker, G.; Goussias, C.; Petrouleas, V.; Rutherford, A. W. *Biochemistry* **2002**, *41*, 3057–3064. (b) Messinger, J.; Seaton, G.; Wydrzynski, T.; Wacker, U.; Renger, G. *Biochemistry* **1997**, *36*, 6862–6873.

(17) Kanady, J. S.; Tran, R.; Stull, J. A.; Lu, L.; Stich, T. A.; Day, M. W.; Yano, J.; Britt, R. D.; Agapie, T. *Chem. Sci.* **2013**, *4*, 3986–3996.

(18) Koumousi, E. S.; Mukherjee, S.; Beavers, C. M.; Teat, S. J.; Christou, G.; Stamatatos, Th. C. *Chem. Commun.* **2011**, *47*, 11128–11130.

(19) For some representative references, see: (a) Zaleski, C. M.; Kampf, J. W.; Mallah, T.; Kirk, M. L.; Pecoraro, V. L. *Inorg. Chem.* **2007**, *46*, 1954–1956. (b) Boron, T. T., III; Kampf, J. W.; Pecoraro, V. L. *Inorg. Chem.* **2010**, *49*, 9104–9106. (c) Zaleski, C. M.; Depperman, E. C.; Kampf, J. W.; Kirk, M. L.; Pecoraro, V. L. *Angew. Chem., Int. Ed.* **2004**, *43*, 3912–3914. (d) Lah, M. S.; Pecoraro, V. L. *J. Am. Chem. Soc.* **1989**, *111*, 7258–7259. (e) Deb, A.; Boron, T. T., III; Itou, M.; Sakurai, Y.; Mallah, T.; Pecoraro, V. L.; Penner-Hahn, J. E. *J. Am. Chem. Soc.* **2014**, *136*, 4889–4892.

(20) (a) Milios, C. J.; Stamatatos, Th. C.; Perlepes, S. P. *Polyhedron* **2006**, *25*, 134–194. (b) Milios, C. J.; Piligkos, S.; Brechin, E. K. *Dalton Trans.* **2008**, 1809–1817. (c) Manoli, M.; Inglis, R.; Manos, M. J.; Nastopoulos, V.; Wernsdorfer, W.; Brechin, E. K.; Tasiopoulos, A. J. *Angew. Chem., Int. Ed.* **2011**, *50*, 4441–4444.

(21) (a) Niko, Y.; Hiroshige, Y.; Kawauchi, S.; Konishi, G. *J. Org. Chem.* **2012**, *77*, 3986–3996. (b) Wu, Y.-Y.; Lu, X.-W.; Qi, M.; Su, H.-C.; Zhao, X.-W.; Zhu, Q.-Y.; Dai, J. *Inorg. Chem.* **2014**, *53*, 7233–7240. (c) Palacios, M. A.; Titos-Padilla, S.; Ruiz, J.; Manuel Herrera, J.; Pope, S. J. A.; Brechin, E. K. *Inorg. Chem.* **2014**, *53*, 1465–1474. (d) Branchi,

B.; Ceroni, P.; Balzani, V.; Klaerner, F. G.; Voegtle, F. *Chem.—Eur. J.* **2010**, *16*, 6048−6055.
(22) Alexandropoulos, D. I.; Mowson, A. M.; Pilkington, M.; Bekiari, V.; Christou, G. *Dalton Trans.* **2014**, *43*, 1965−1969.
(23) Kottke, T.; Stalke, D. *J. Appl. Cryst.* **1993**, *26*, 615−619.
(24) *APEX2,* Data Collection Software Version 2.1-RC13; Bruker AXS: Delft, The Netherlands, 2006.
(25) *Cryopad,* Remote Monitoring and Control, Version 1.451; Oxford Cryosystems: Oxford, U.K., 2006.
(26) *SAINT+,* Data Integration Engine v. 7.23a; Bruker AXS: Madison, WI, 1997−2005.
(27) *CrysAlis*^{Pro} Software Package, Version 1.171; *Xcalibur Single Crystal CCD Diffractometer,* Oxford Diffraction (Agilent): Santa Clara, CA.
(28) Sheldrick, G. M. *SADABS v.2.01,* Bruker/Siemens Area Detector Absorption Correction Program; Bruker AXS: Madison, WI, 1998.
(29) Sheldrick, G. M. *SHELXS-97,* Program for Crystal Structure Solution; University of Göttingen: Göttingen, Germany, 1997.
(30) Sheldrick, G. M. *Acta Crystallogr., Sect. A* **2008**, *64*, 112−122.
(31) Sheldrick, G. M. *SHELXL-97,* Program for Crystal Structure Refinement; University of Göttingen: Göttingen, Germany, 1997.
(32) (a) Spek, A. L. *J. Appl. Crystallogr.* **2003**, *36*, 7−13. (b) van der Sluis, P.; Spek, A. L. *Acta Crystallogr., Sect. A* **1990**, *46*, 194−201.
(33) (a) Mercury; Bruno, I. J.; Cole, J. C.; Edgington, P. R.; Kessler, M. K.; Macrae, C. F.; McCabe, P.; Pearson, J.; Taylor, R. *Acta Crystallogr., Sect. B* **2002**, *58*, 389−397. (b) Bradenburg, K. *DIAMOND,* Release 3.1f; Crystal Impact GbR: Bonn, Germany, 2008.
(34) Bain, G. A.; Berry, J. F. *J. Chem. Educ.* **2008**, *85*, 532−536.
(35) (a) Tsui, E. Y.; Kanady, J. S.; Agapie, Th. *Inorg. Chem.* **2013**, *52*, 13833−13848. (b) Kanady, J. S.; Mendoza-Cortes, J. L.; Tsui, E. Y.; Nielsen, R. J.; Goddard, W. A., III; Agapie, Th. *J. Am. Chem. Soc.* **2013**, *135*, 1073−1082.
(36) (a) Tasiopoulos, A. J.; Wernsdorfer, W.; Abboud, K. A.; Christou, G. *Angew. Chem., Int. Ed.* **2004**, *43*, 6338−6342. (b) King, P.; Wernsdorfer, W.; Abboud, K. A.; Christou, G. *Inorg. Chem.* **2005**, *44*, 8659−8669.
(37) Khairy, E. M.; Shoukry, M. M.; Khalil, M. M.; Mohamed, M. M. A. *Transition. Met. Chem.* **1996**, *21*, 176−180. (b) Hall, M. D.; Failes, T. W.; Hibbs, D. E.; Hambley, T. W. *Inorg. Chem.* **2002**, *41*, 1223−1228.
(38) (a) Deacon, G. B.; Phillips, R. J. *Coord. Chem. Rev.* **1980**, *33*, 227−250. (b) Stamatatos, Th. C.; Raptopoulou, C. P.; Perlepes, S. P.; Boudalis, A. K. *Polyhedron* **2011**, *30*, 3026−3033.
(39) Glazunov, V. P.; Mashkovsky, A. A.; Odinokov, S. E. *J. Chem. Soc., Faraday Trans. 2* **1979**, *75*, 629−635.
(40) Cinco, R. M.; Holman, K. L. M.; Robblee, J. H.; Yano, J.; Pizarro, S. A.; Bellacchio, E.; Sauer, K.; Yachandra, V. K. *Biochemistry* **2002**, *41*, 12928−12933.
(41) (a) Messinger, J.; Robblee, J. H.; Bergmann, U.; Fernandez, C.; Glatzel, P.; Visser, H.; Cinco, R. M.; McFarlane, K. L.; Bellacchio, E.; Pizarro, S. A.; Cramer, S. P.; Sauer, K.; Klein, M. P.; Yachandra, V. K. *J. Am. Chem. Soc.* **2001**, *123*, 7804−7820. (b) Solomon, E. I.; Hedman, B.; Hodgson, K. O.; Dey, A.; Szilagyi, R. K. *Coord. Chem. Rev.* **2005**, *249*, 97−129.
(42) For an excellent review on metallacrowns and their nomenclature, see: Pecoraro, V. L.; Stemmler, A. J.; Gibney, B. P.; Bodwin, J.; Kampf, J. W.; Wang, H. Metallacrowns: A New Class of Molecular Recognition Agents. In *Progress in Inorganic Chemistry;* Karlin, K., Ed.; Wiley: Hoboken, NJ, 1996; Vol. *45*, p 83.
(43) Addison, A. W.; Rao, T. N.; Reedijk, J.; Rijn, J.; Verschoor, G. C. *J. Chem. Soc., Dalton Trans.* **1984**, 1349−1356.
(44) Liu, W.; Thorp, H. H. *Inorg. Chem.* **1993**, *32*, 4102−4105.
(45) Zabrodsky, H.; Peleg, S.; Avnir, D. *J. Am. Chem. Soc.* **1993**, *115*, 8278−8289.
(46) Alvarez, S.; Alemany, P.; Casanova, D.; Cirera, J.; Llunell, M.; Avnir, D. *Coord. Chem. Rev.* **2005**, *249*, 1693−1708.
(47) Schwarz, F. P.; Wasik, S. P. *Anal. Chem.* **1976**, *48*, 524−528.
(48) Lever, A. B. P. *Inorganic Electronic Spectroscopy;* Elsevier: Amsterdam, 1997.
(49) (a) Qi, Z.; Heinrich, T.; Moorthy, S.; Schalley, C. A. *Chem. Soc. Rev.* **2015**, in press. DOI: 10.1039/c4cs00167b. (b) Winter, R. S.; Yan, J.; Busche, C.; Mathieson, J. S.; Prescimone, A.; Brechin, E. K.; Long, D.-L.; Cronin, L. *Chem.—Eur. J.* **2013**, *19*, 2976−2981. (c) Mazarakioti, E. C.; Poole, K. M.; Cunha-Silva, L.; Christou, G.; Stamatatos, Th. C. *Dalton Trans.* **2014**, *43*, 11456−11460.
(50) (a) Bagai, R.; Christou, G. *Inorg. Chem.* **2007**, *46*, 10810−10818. (b) Soler, M.; Wernsdorfer, W.; Abboud, K. A.; Huffman, J. C.; Davidson, E. R.; Hendrickson, D. N.; Christou, G. *J. Am. Chem. Soc.* **2003**, *125*, 3576−3588.
(51) Bagai, R.; Christou, G. *Chem. Soc. Rev.* **2009**, *38*, 1011−1026.
(52) (a) Rappaport, F.; Ishida, N.; Sugiura, M.; Boussac, A. *Energy Environ. Sci.* **2011**, *4*, 2520−2524. (b) Tsui, E. Y.; Agapie, Th. *Proc. Natl. Acad. Sci. U. S. A.* **2013**, *110*, 10084−10088.
(53) (a) Kulik, L. V.; Epel, B.; Lubitz, W.; Messinger, J. *J. Am. Chem. Soc.* **2007**, *129*, 13421−13435. (b) Randall, D. W.; Sturgeon, B. E.; Ball, J. A.; Lorigan, G. A.; Chan, M. K.; Klein, M. P.; Armstrong, W. H.; Britt, R. D. *J. Am. Chem. Soc.* **1995**, *117*, 11780−11789.
(54) Sessoli, R.; Tsai, H.-L.; Schake, A. R.; Wang, S.; Vincent, J. B.; Folting, K.; Gatteschi, D.; Christou, G.; Hendrickson, D. N. *J. Am. Chem. Soc.* **1993**, *115*, 1804−1816.
(55) Eppley, H. J.; Tsai, H.-L.; de Vries, N.; Folting, K.; Christou, G.; Hendrickson, D. N. *J. Am. Chem. Soc.* **1995**, *117*, 301−317.
(56) Chia, Y. Y.; Tay, M. G. *Dalton Trans.* **2014**, *43*, 13159−13168 (Perspective).
(57) (a) Fleischauer, P. D.; Fleischauer, P. *Chem. Rev.* **1970**, *70*, 199−230 and references cited therein. (b) de Silva, A. P.; Gunaratne, H. Q. N.; Gunnlaugsson, T.; Huxley, A. J. M.; McCoy, C. P.; Rademacher, J. T.; Rice, T. E. *Chem. Rev.* **1997**, *97*, 1515−1566.
(58) (a) Glorius, M.; Moll, H.; Bernhard, G. *Polyhedron* **2008**, *27*, 2113−2118. (b) Weng, J.-H.; Shieh, Y.-J. *Photosynth. Res.* **2004**, *82*, 151−164.
(59) (a) Schawrz, F. P.; Wasik, S. P. *Anal. Chem.* **1976**, *48*, 524−528. (b) Uchida, K.; Takahashi, Y. *Int. J. Quantum Chem.* **1980**, *18*, 301−305.
(60) (a) Zhang, J.; Lee, J.-K.; Wu, Y.; Murray, R. W. *Nano Lett.* **2003**, *3*, 403−407. (b) Zhu, L.; Al-Kaysi, R. O.; Dillon, R. J.; Tham, F. S.; Bardeen, C. J. *Cryst. Growth Des.* **2011**, *11*, 4975−4983. (c) Alberding, B. G.; Brown-Xu, S. E.; Chisholm, M. H.; Gustafson, T. L.; Reed, C. R.; Naseri, V. *Dalton Trans.* **2012**, *41*, 13097−13104. (d) Al-Kaysi, R. O.; Bardeen, C. J. *Adv. Mater.* **2007**, *19*, 1276−1280. (e) Khanra, P.; Kuila, T.; Bae, S. H.; Kim, N. H.; Lee, J. H. *J. Mater. Chem.* **2012**, *22*, 24403−24410. (f) Beedle, C. C.; Stephenson, C. J.; Heroux, K. J.; Wernsdorfer, W.; Hendrickson, D. N. *Inorg. Chem.* **2008**, *47*, 10798−10800.
(61) (a) Winnik, F. M. *Chem. Rev.* **1993**, *93*, 587−614. (b) Hu, J.-Y.; Yamato, T. Synthesis and Photophysical Properties of Pyrene-Based Light-Emitting Monomers: Highly Blue Fluorescent Multiply-Conjugated-Shaped Architectures. In *Organic Light Emitting Diode—Material, Process and Devices;* Ko, S. H., Ed.; InTech: Rijeka, Croatia, 2011.
(62) (a) Duhamel, J. *Langmuir* **2012**, *28*, 6527−6538. (b) Seko, T.; Ogura, K.; Kawakami, Y.; Sugino, H.; Toyotama, H.; Tanaka, J. *Chem. Phys. Lett.* **1998**, *291*, 438−444.
(63) Chilton, N. F.; Anderson, R. P.; Turner, L. D.; Soncini, A.; Murray, K. S. *J. Comput. Chem.* **2013**, *34*, 1164−1175.
(64) For example, see: (a) Koumousi, E. S.; Raptopoulou, C. P.; Perlepes, S. P.; Escuer, A.; Stamatatos, Th. C. *Polyhedron* **2010**, *29*, 204−211. (b) Pringouri, K. V.; Raptopoulou, C. P.; Escuer, A.; Stamatatos, Th. C. *Inorg. Chim. Acta* **2007**, *360*, 69−83. (c) Verani, G. N.; Bothe, E.; Burdinski, D.; Weyhermüller, T.; Flörke, U.; Chaudhuri, P. *Eur. J. Inorg. Chem.* **2001**, 2161−2169. (d) Gass, I. A.; Milios, C. J.; Collins, A.; White, F. J.; Budd, L.; Parsons, S.; Murrie, M.; Perlepes, S. P.; Brechin, E. K. *Dalton Trans.* **2008**, 2043−2053.
(65) (a) Béck, W. F.; Brudvig, G. W. *Biochemistry* **1987**, *26*, 8285−8295. (b) Lin, C.; Brudvig, G. W. *Photosynth. Res.* **1993**, *38*, 441−448. (c) Riggs-Gelasco, P. J.; Mei, R.; Yocum, C. F.; Penner-Hahn, J. E. *J. Am. Chem. Soc.* **1996**, *118*, 2387−2399.

(66) (a) Sarrou, J.; Ioannidis, N.; Deligiannakis, Y.; Petrouleas, V. *Biochemistry* **1998**, *37*, 3581−3587. (b) Ioannidis, N.; Sarrou, J.; Schansker, G.; Petrouleas, V. *Biochemistry* **1998**, *37*, 16445−16451.
(67) (a) Messinger, J.; Wacker, U.; Renger, G. *Biochemistry* **1991**, *30*, 7852−7862. (b) Bösing, P.; Willner, A.; Pape, T.; Heppa, A.; Mitzel, N. W. *Dalton Trans.* **2008**, 2549−2556. (c) Kuntzleman, T.; Yocum, C. F. *Biochemistry* **2005**, *44*, 2129−2142.